

Project Number: DJO -0208

Experimental Study of Parachute Suspension Line Drag

A Major Qualifying Project Report

Submitted to the Faculty of the

WORCESTER POLYTECHNIC INSTITUTE

in partial fulfillment of the requirements for the

Degree of Bachelor of Science

in Mechanical Engineering

by

Stephen Black

Boris Mandadzhiev

Amanda Thompson

Date Submitted:

Approved:

Prof. David J. Olinger

Abstract

The drag force created by suspension lines on a parachute system can often be a large part of the total aerodynamic drag of the system. For parafoils, parachute systems with a high glide ratio, the suspension line drag can result in a reduction of the glide ratio and overall degradation in the parachute system performance.

This project was completed on-campus at WPI, with collaboration from engineers from the project sponsor, the U.S. Army Natick Soldier Center. The report describes wind tunnel testing of parachute suspension line drag that was undertaken. An experimental apparatus to measure suspension line drag was designed and constructed. Wind tunnel tests were carried out for a variety of suspension lines, different line orientations, line tensions, and wind tunnel speeds. Dimensional analysis was completed to determine the important non-dimensional parameters for the problem. Instantaneous drag data was analyzed using Fast Fourier Transfer to determine the frequency response of the suspension lines. Mean drag data was also measured and analyzed.

Acknowledgments

There are many individuals whose help was essential to the completion of this project. Specifically, a special thank you is given to the members of the Natick community who donated time and resources to this project: Dr. Ken Desabrais, Dr. Jose Miletti, and Dr. Calvin Lee. We would also like to express our appreciation to Adriana Hera for the enormous contribution she has provided us throughout the entire project. Thank you to Neil Whitehouse for explaining and assisting with the construction of materials for the wind tunnel. To our project advisor, Professor David Olinger, thank you for facilitating our project and supervising our work. Without your help, the project would not have been possible. Thank you.

Table of Contents

Abstract	i
Acknowledgments	ii
Table of Contents	iii
List of Tables	v
List of Figures	v
I. Introduction	1
II. Background.....	3
II.1 Round vs. Ram-air Parachutes	3
II.2 PADS Development	4
II.3 Project Objectives	6
III. Design	7
III.1 Design Specifications and Constraints.....	7
III.2 Development.....	9
III.3 Line Tensioning Apparatus.....	3
III.3.1 Tensioning Mechanism	3
III.3.2 Load Cell Integration.....	4
III.4 Data Acquisition.....	6
III.5 Final Design.....	9
III.6 Dimensional Analysis	10
III.6.1 Equivalent Resonant Frequency	10
III.6.2 MC-4 Prototype Specifications.....	14
III.6.3 Vortex Shedding	15
III.7 Calculations	19
IV. Testing Methodology	23
IV.2 DAQ Equipment Setup	23
IV.1 Apparatus Setup.....	24
IV.3 Bias Testing	26
IV.4 Drag Testing	27
IV.5 Data Extraction	27
V. Results and Analysis	29
VI. Conclusions	32
VII. Recommendations	33
References.....	35
Appendices.....	36
Appendix A - S-Beam Junior Load Cell.....	36
Appendix B – Line Stretch Testing.....	37
Appendix C – Wind Tunnel Specifications	40
Appendix D – Transducer Specifications	41
Appendix E - Transducer Certificate of Calibration	43
Appendix F - Transducer – to – Tensioning Arm Plate.....	44
Appendix G – Tensioning Structure	45
Appendix H – Project Timeline.....	46
Appendix I – Final Experimental Matrix.....	47

Appendix J – Mean Drag Data	48
Appendix K – 80/20 Aluminum Extrusions	49
Appendix L – MC-4 Parachute Technical Specifications	54
Appendix M – WPICConversion08.m MATLAB code	55
Appendix N – ATIDaqFT_Convert2.m MATLAB code	56
Appendix O – NEW_MQP_FFT.m MATLAB code	58

List of Tables

Table 1: MC-4 Suspension Line Properties	16
------------------------------------------------	----

List of Figures

Figure 1: Standard Ram-air Parachute (6)	4
Figure 2: Typical PADS (6)	5
Figure 3: Preliminary Design.....	8
Figure 4: Conceptual Design in SolidWorks	9
Figure 5: Cross Section of 80/20 Aluminum Extrusion.....	10
Figure 6 - SolidWorks Design	11
Figure 7: Six Axis Transducer	11
Figure 8: Back Plate and Circular Mount	11
Figure 9 - Calibration and Alignment	2
Figure 10: Calibration and Alignment	2
Figure 11 - CNC Machined Plug.....	3
Figure 12: Solid Computer Model.....	3
Figure 13: Tensioning Mechanism.....	3
Figure 14: Load Cell	4
Figure 15 - Load cell Calibration Curve	5
Figure 16 - Load cell power supply.....	6
Figure 17: DAQ System Setup	6
Figure 18 - LabView 8.2 VI.....	7
Figure 19 - Block Diagram	8
Figure 20: Final Structure Design	9
Figure 21 - Line Resonant Frequency vs. Tension.....	16
Figure 22 - Vortex Shedding Frequency vs. Wind Speed	17
Figure 23 - Tension vs. Wind Speed	18
Figure 24 - Re vs. Wind Speed.....	19
Figure 25 - Re vs. Line Diameter, V=10m/s.....	19
Figure 26 - Drag Coefficient vs. Re (9)	20
Figure 27 - Drag Force vs. Line Diameter, V=10m/s	21
Figure 28 - Drag force vs. Wind Speed, d=0.3 m.....	21
Figure 29 – DAQ Connection diagram	23
Figure 30: ATI DAQ F/T Demo Software User Interface	24
Figure 31 - Support structure alignment	25
Figure 32: Circular Mount Attached to the Back Plate.....	25
Figure 33 - Last assembly step	26
Figure 34 - From raw voltages to filtered forces and torques.....	27
Figure 35: Raw drag data: Low frequency noise.....	29
Figure 36: Raw drag data: High frequency noise	30
Figure 37: Drag data FFT.....	30
Figure 38: FFT for Low Frequency Response.....	31
Figure 39: Vibration Frequency Response for Windspeeds 6, 8, 10, and 12 m/s	31

I. Introduction

The goal of this project was to conduct an experimental study of parachute suspension line drag. Using the WPI closed circuit wind tunnel, the project focused on developing analysis tools, testing the suspension line drag on a variety of arrangements, and analyzing the data using Fourier analysis.

The first parachute-like device for an airplane was patented in 1920, based on the sketches of Da Vinci. It allowed for a low-impact landing after ejecting from an airplane mid-flight. This device used a fabric canopy that attached to a harness around an individual, thus slowing the rate of descent and allowing for a safe fall from extreme heights. According to the inventor, Karl O. K. Osterday, “one object of the present invention is to provide a...means of which the aviator can release himself from his wrecked machine, while in the air, and make a safe landing (1).” While the initial parachute design was appropriate for the early 20th century, the needs of today’s parachutes are much greater.

Current parachute systems have higher demands and require a large array of capabilities. For example, the T-10 parachute system was widely used since the 1950s for military procedures. Recently, the system became a liability to the men and women using it, and in 2001 the extra weight from larger and more equipped soldiers was deemed to be too heavy for the parachute (2). Even though engineers continue to use high-quality testing facilities and advanced technology in their current parachute design, there is still room for improvement.

Since 1954, The US Army Natick Soldier Research, Development and Engineering Center (NSRDEC), based out of Natick, MA, has focused on developing the basic materials used by the U.S. Army. The center provides technological assistance to the military and strives to aid local civilian operations. Well known for their work, the Natick Soldier Center – Army R&D Laboratory has won Lab of the Year for five of the last six years. This project was conducted with the NSRDEC. Dr. Ken Desabrais and Dr. Jose Miletti of the NSRDEC served as technical consultants and advisors to the project.

The mission of the NSRDEC is to “maximize the warrior’s survivability, sustainability, mobility, combat effectiveness and quality of life by treating the warrior as

a system (3).” The soldier center employs over 2,000 individuals, including civilians, military personnel and contractors. Having a combined annual budget of over \$1 billion, they are continually envisioning and producing technologically advanced items.

One component of the NSRDEC is Airdrop and Aerial Delivery, working “to conduct research and engineering in military parachuting and airdrop systems to increase aircraft/airborne force survivability; improve airdrop accuracy and functional reliability; reduce personnel injuries/casualties; and lower the cost to develop, produce and maintain these complex systems (4).”

As parachutes continue to develop into more complex entities, greater control over the system must be established. One particular area the NSRDEC has researched is the horizontal drag on ram-air type parachutes. If the parachute’s drag can be reduced, the military will have more control over its route and landing. Large amounts of research have been put into creating more aerodynamic and parafoil-like designs, resulting in highly maneuverable parachutes such as the MC-4 and Mega-fly.

It is becoming even more necessary to reduce the horizontal drag forces on parachutes as their operations become increasingly demanding. As the military mission becomes more specific, it is essential for the system to be controlled. For example, if a computer is guiding the parachute to a certain location, less drag will allow for a more effective glide ratio. This will enable the system to have more time for maneuvers to reach the specified site.

In recent years, the NSRDEC has begun researching parachute suspension lines as a source of drag. It has been theorized that up to 40% of horizontal drag on ram-air parachutes can be attributed to the suspension lines (5). Although theories on the mechanisms behind suspension line drag have been made, there remains a lack of supporting experimental data. If information can be provided on the aerodynamic drag of current suspension lines, improvements can be implemented to develop improved parachute recovery systems.

II. Background

II.1 Round vs. Ram-air Parachutes

The U.S. Army utilizes many variations of the basic parachute structure in use today. Variants of the parachute recovery system include low glide and high glide parachutes, also known as round and ram-air parachutes. Ideally, every parachute system would have high accuracy while withstanding heavy payloads; this, however, is generally not the case.

The round parachute is mainly a dome-shaped, cloth canopy. The parachute does not act in a similar manner to an airfoil because no lift forces are applied to the device. Not as maneuverable as a ram-air parachute, the round parachute can be steered thanks to a specific design capability. Air is released through the back of the main canopy, slowing its speed. The decrease in velocity allows for the mechanism to be guided in a variety of directions. The round parachute can also be clustered, holding payloads of up to 60,000 lb (5). Due to the substantial payload, the round parachute's primary use is heavy payload drops as opposed to personnel parachutes. Since this parachute has less control and heavier loads, it is difficult to have it fall accurately.

The Ram-air parachute (Fig. 1), also known as a parafoil system, is generally used as a personnel parachute however other methods of use are discussed below. The airfoil self-inflates and creates an airfoil shape that allows for the direction and speed of the apparatus to be controlled by the accompanying individual. It does this by having two separate sheets of fabric, shaped into long cells. The parachute does not generally sustain the weight of more than one individual. For example, the standard freefall parachute is the MC-4 Ram Air parachute (6).

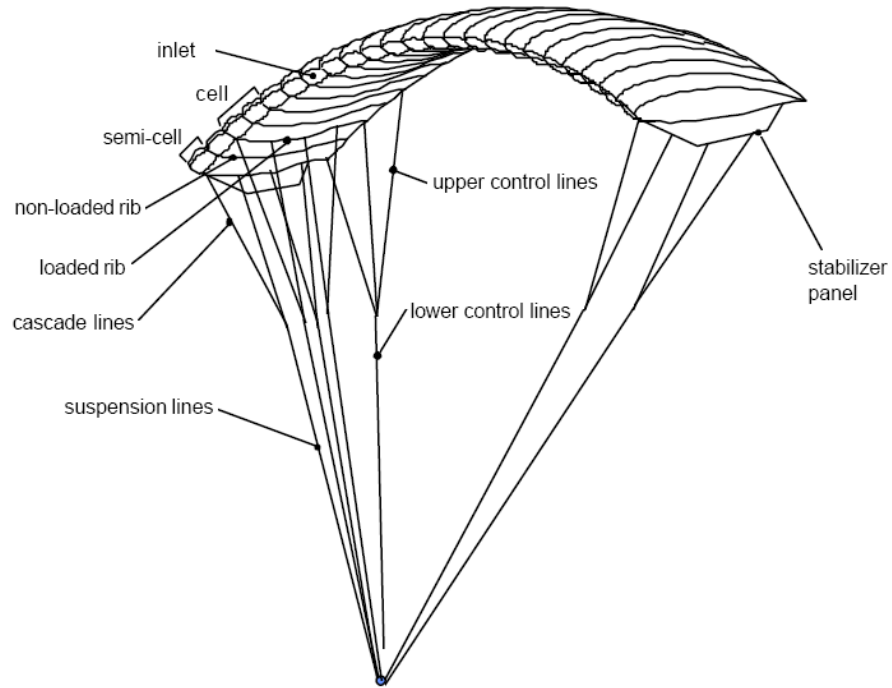


Figure 1: Standard Ram-air Parachute (6)

There are many varieties of Ram-air parachutes. As mentioned above, the MC-4 Ram Air Free-Fall parachute is one of the standard pieces of equipment used in the military. It is made of seven cells and is designed to be user-friendly allowing for individual adjustments and equipment storage (7).

II.2 PADS Development

In recent years, the military has begun focusing on accurate delivery of equipment and supplies using Ram-air parachutes. These missions are known as Precision Aerial Delivery System (PADS) missions. These systems are controlled by onboard GPS navigation systems as depicted below.

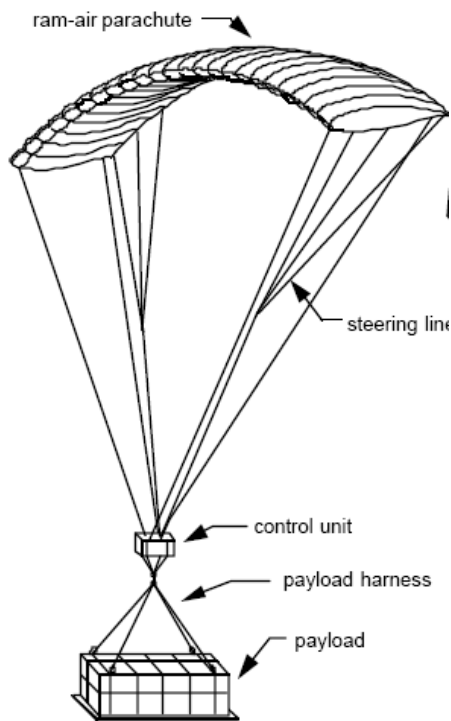


Figure 2: Typical PADS (6)

There are many requirements for a PADS mission. The statistics and objectives listed below are a few of the restrictions described in the “Precision Aerial Delivery Seminar Ram-Air Parachute Design” written by J. Stephen Lingard.

- Deployment altitude: up to 35,000 ft
- Offset range: up to 20 km
- Accuracy: < 100 m from planned delivery point
- Suspended mass: 225 kg - 19,000 kg
- Soft landing desired
- Predictable high glide ratio
- Predictable flight speeds
- The ability to flare to reduce landing speed

The stringent needs of these missions provide an even greater reason to have a full understanding of the aerodynamic drag on ram-air parachutes.

II.3 Project Objectives

The purpose of this project was to examine the aerodynamics of parachute suspension lines through experimental studies. Specifically, the effects of certain line characteristics such as surface roughness, line orientation, and flexibility of the line on line drag were studied. We developed our goal by completing the objectives created during the initial stages of the project and by following the process described in the Methodology. Our objectives were as follows:

- Research current suspension line arrangements.
- Develop analysis tools for the aerodynamic characteristics of suspension line arrangements.
- Design and construct an experimental apparatus capable of measuring suspension line drag in the WPI closed-circuit wind tunnel.
- Conduct wind tunnel tests to measure line drag on a variety of suspension lines, different line orientations, line tensions, and wind speeds based upon dimensional analysis.
- Analyze the test data using Fourier analysis tools.
- Compare analysis results with the wind tunnel data.

III. Design

The design process stemmed from a previously built apparatus and six-axis force-moment transducer provided by the US Army Natick Soldier Center. The devices had previously been used to measure drag forces in a wind and water tunnels. The combination of the chosen sensor and the support structure directed the new design process towards a structure mounted on top of the wind tunnel which utilized an external U-shaped tensioning arm and measured torque and force created by line drag on two of the sensing axes of the transducer. A load cell was also used to measure and control the tension on the line incorporated in the design.

III.1 Design Specifications and Constraints

The following is a list of constraints that the design needed to follow:

1. The parachute suspension line should be the only entity in the test section of the wind tunnel. Thus, no flow disturbances are introduced that could eventually offset the results from the true values.
2. Because of the direct correlation between line tensions and oscillations of the line, a tensioning mechanism is required to reflect the tension on the tested specimen.
3. The entry point of the tested line into the test section must be sealed by some means, while still providing clearance for induced vibrations of the line and rotation of the line around the Z (vertical) axis to achieve different angles with respect to the oncoming flow.
4. A lightweight tensioning arm to hold the specimen is required. This is needed since the tensioning arm is connected to one of the sensing axis of the six-axis transducer which has an upper limit of mass it can support.
5. An adequate way of positioning the entire setup is needed in order to avoid misplacement of the structure and thus discrepancy in the results. Structure should be easily aligned and calibrated.

6. Calibration methodology and ability of the setup is required to make it possible to align desired transducer axis with forces acting on the test specimen so that no forces would be resolved in components making it much easier to analyze.
7. To understand the results of the conducted experiments an adequate data collections system is required.
8. Rigid structure – so that all force components are translated to the sensing device with minimal dampening.

The final wind tunnel setup was composed of two rigid structures and two force transducers as depicted below:

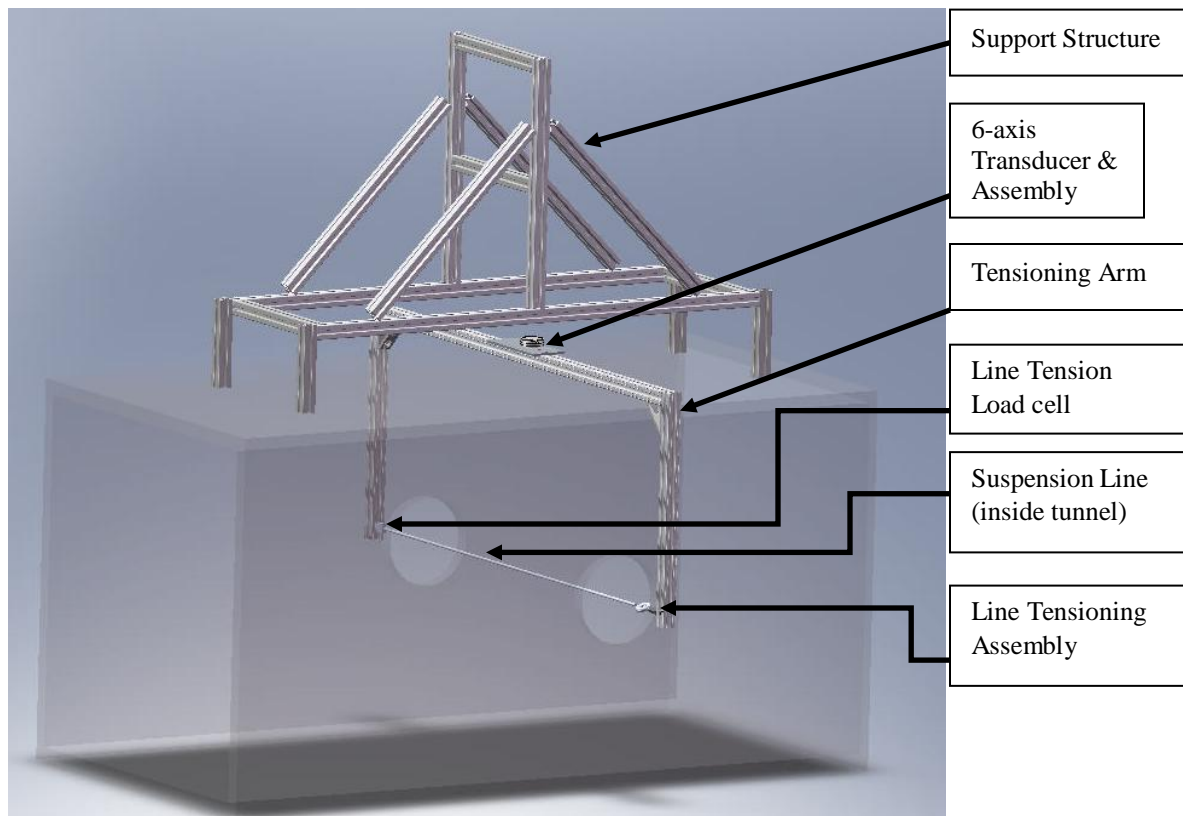


Figure 3: Preliminary Design

The support structure, transducer, and load cell were provided by the US Army Natick Soldier Center. All other components were bought, built, or machined.

III.2 Development

The WPI closed circuit wind tunnel (for details on wind tunnel specifications see App. C) to be used for this project has a square 2 by 2 feet test section. For the most accurate data to be obtained the flow inside the test section must be uniform and free from disturbances. The introduction of any device would cause flow fluctuations which may have undesirable and unpredicted impact on the aerodynamic characteristics of the tested object. Clearly an external sensing device (Fig. 4) is preferable, causing no flow disturbances. In consideration of this design many complexities have to be addressed.

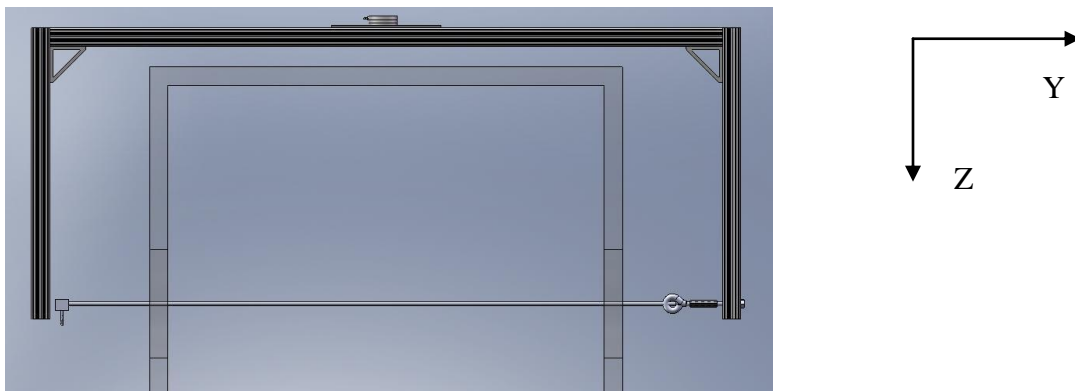


Figure 4: Conceptual Design in SolidWorks

The air flow created by the wind tunnel is normal to the page in Figure 4 creating drag force on the line. Measuring this force is not a trivial task because of the fact that the sensing unit (six axis sensor) is placed between the tensioning arm and the support structure. This offset from the line of the drag force creates a moment which has the magnitude of the drag force multiplied by the moment arm.

Other possibilities have been considered to construct the test apparatus. One involved placing the sensing devices on the line of the drag action force. The design would use rails to be placed on the side of the wind tunnel walls and be virtually frictionless. This way no twisting of the structure occurs, no apparatus is inside the test section of the wind tunnel and no magnification effect of the small forces can occur as it would in the case with the torque. This design was discarded because of unaccounted benefits compared to cost and longer design time associated with the frictionless rails.

Two of the requirements concerning the tensioning arm are that it should be both lightweight and stiff. We have managed to achieve this by using aluminum sections as the frame of the structure. These are 80/20 aluminum extrusions with specific cross sections for enhanced moment of inertias and low density per length (see App K for details).

Part No.	1004
Material	6105-T5
Finish	Clear Anodized
Weight Per Foot	.5609 Lbs.
Stock Length (+/- .125")	145" - Part No. 1004-145 242" - Part No. 1004-242
Moment Of Inertia	IX=.0443 ⁱⁿ ⁴ IY=.0541 ⁱⁿ ⁴
Estimated Area	.4819 Sq. In.

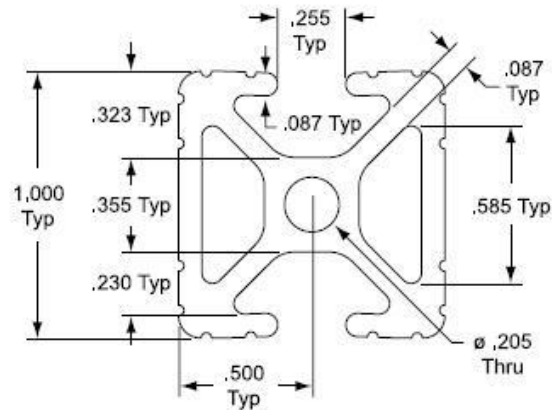


Figure 5: Cross Section of 80/20 Aluminum Extrusion

The support structure, built using 80/20 aluminum extrusions as well, on which we would mount our drag sensing device – tensioning arm and sensor, was previously used for a number of testing setups including variable angle of attack in water tunnel testing. Thus this setup has proven to be useful and working for the type of experiments we would be conducting. Apart from the fact that it was given to the project by the R&D Center in Natick it is perfectly suitable for use on the wind tunnel available to us. It is very stiff and only slight modifications were needed to fit in our design.

The ‘yoke’, which we will call the tensioning arm, would connect to the already existing setup at a single point. In order for any forces or torques to be detected by the force-torque sensor the structure should not be in contact with any other objects. The only point of connection between the two structures is where they connect to the transducer. Thus, the flexing point is in the sensing device rather than anywhere on this arm. Initial dimensional analysis (discussed in Methodology) of different velocities and tensions showed that the line tension may need to be as high as 20 lb. Therefore the loads that the tensioning arm had to sustain over the entire length of 39 inches may cause significant

deflections at the midsection of the arm. This is a concern for two reasons. One is the fact that after tensioning the specimen to the desired tension, the bend created may have change the overall shape of the tensioning arm which is not desirable. Also, the bending that may get created at the midsection of the arm may be enough to cause damage to the six axis transducer. A SolidWorks/COSMOS simulation was run to show maximum bending. Even though the analysis showed no extreme deflections a decision was made not to attach the transducer directly to the tensioning arm, but rather to use a steel plate in between for additional stiffness at the maximum bending point.

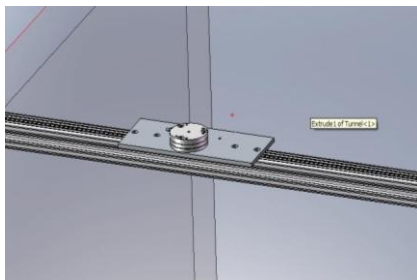


Figure 6 - SolidWorks Design



Figure 7: Six Axis Transducer



Figure 8: Back Plate and Circular Mount

The assembly had to be adjustable so that it would accommodate any imperfections or misalignments in the rest of the setup. The side arms are free to slide to the desired position and at the same time being able to attach securely to the rest of the setup via a 4 hole inside gusset corner bracket (Appendix K).

We are also interested in the vibrations created by the suspension line and the corresponding drag. A dimensional analysis shows that controlled variables should be

tension on the line and free stream velocity. The combination of the two would cause a different vortex shedding pattern which may result in a different drag on the line.

To control the tension on the line a load cell (strain gauge in its nature) together with a simple tensioning mechanism is used. The free stream velocity is controlled by the wind tunnel control panel.

Since the support structure is free to move once on the top panel of the wind tunnel a calibration methodology was developed to ensure perfect alignment with the transducer axes so that no force/torque component build up occurs.



Figure 9 - Calibration and Alignment

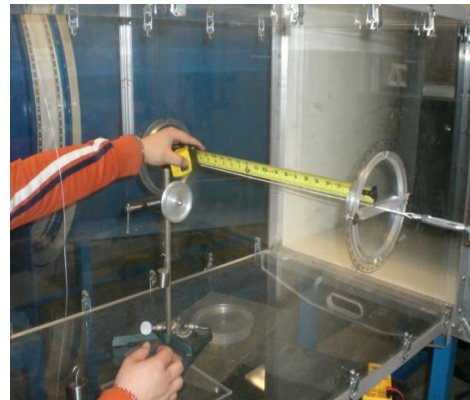


Figure 10: Calibration and Alignment

Furthermore, to add the load cell and tensioning assembly additional spacing between the wind tunnel walls and the support beams had to be accounted for adding to the overall length.

Access to the test section of the wind tunnel is through port holes on each wall. The portholes are sealed by plugs specially manufactured for different experiments. Even though previous designs of plugs are available to us, new ones designed specifically for our testing purposes are needed. The plugs are designed so that enough room exists between the test specimen and the slots through which the line enters the wind tunnel test section and at the same time maintaining good seal. Enough spacing is required because of the vortex shedding induced vibrations of the line which may cause significant amplitudes. Furthermore, the slots allow for the line to be placed at different angles to the free stream in the horizontal plane.

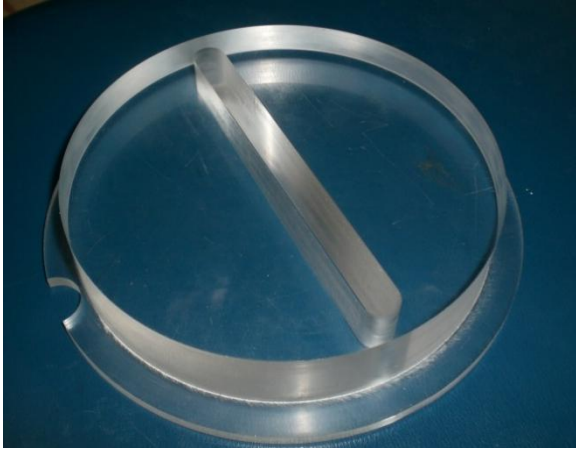


Figure 11 - CNC Machined Plug

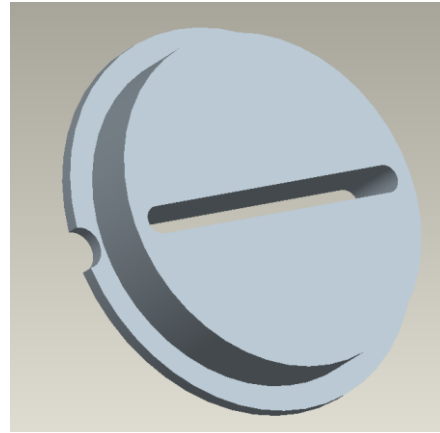


Figure 12: Solid Computer Model

III.3 Line Tensioning Apparatus

III.3.1 Tensioning Mechanism

The tensioning of the parachute line needed to be measured accurately. In order to do this, the group developed various tensioning mechanism concepts. Initial concepts included weights, pulley systems, and compressed air pistons.

To incorporate the tensioning mechanism with the tensioning arm $\frac{1}{4}$ - 20 size holes had to be drilled through the aluminum extrusions. In the current design we use $\frac{1}{4}$ -20 threaded bolts to hold the load cell and the tensioning assembly (see Fig. 13). Adjusting the tension on the test specimen is done by screwing the $\frac{1}{4}$ - 20 bolt in the hook assembly. This is done by hand since the required tensions are small. However, if higher tensions are needed a wrench can be used to turn the $\frac{1}{4}$ - 20 bolt.



Figure 13: Tensioning Mechanism

III.3.2 Load Cell Integration

The mechanism chosen to measure line tension uses the Futek Model LSB200 (L2357) S-Beam Junior Load Cell (6). The load cell was “designed for inline loading in tension and compression.” In the case of our project, the load cell will be used for measuring the tension of the line when it is placed inside the wind tunnel. The load cell’s small size along with its ability to accurately measure loads up to 100 pounds makes it ideal for this project. With its small size and light weight the load cell does not hinder the measurements of the project. The accuracy of the instrument has minimal error with a nonlinearity of $\pm 0.1\%$. The design is simple – the load cell connects directly to one of the sides of the tensioning arm and to the test specimen. The tensioning mechanism connects on the other side of the wind tunnel to the tensioning arm as well and consists of a hook assembly and a $\frac{1}{4}$ - 20 bolt.



Figure 14: Load Cell

Initially the load cell had the purpose of not only indicating the tension on the line but also to sense any flow induced vibrations created by the vortex shedding. A high sampling rate is required to sense the estimated frequencies. Using LabView and the DAQ computer, provided to us by the Research center at Natick, proved to work with the load cell assembly. However, an unknown event caused the setup to malfunction and not output data. No solution was found to this problem. Acquiring data from the Load Cell is done using a DMM (digital volt meter) to measure the output voltage. A calibration curve has been established to correlate voltage outputs to real tensions (Fig – 15). We used standards listed below with a known mass hanging from the load cell to build the calibration curve. Developed a curve fit equation to correlate raw voltages to weights. This is needed because in order to tension a line to a specific tension a certain volt output should be achieved. Using this equation and supplying it with the desired tension we

were able to obtain the corresponding voltage our load cell should output. A unit conversion for the tensions to pounds was necessary since only metric weights were available to us.

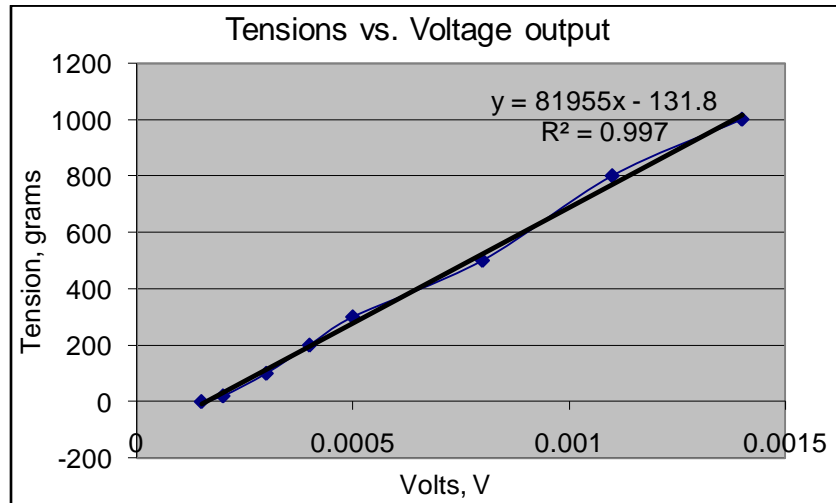


Figure 15 - Load cell Calibration Curve

Because of a failure of the DAQ channel acquiring load cell output the use of a Digital Multi Meter (DMM) was introduced as a solution. The resolution of the DMM is considerably lower than that of the DAQ PCI Card in the computer. The maximum resolution in the volts range is 0.1 mV which is enough to be used as low voltage output reader.

The power need for the load cell is +/- 10V. The selection of the power supply is of great importance since the output of the load cell is proportional to the power input. Any disturbances in input voltage will be reflected at the output which causes discrepancy between true measured values and load cell actual output. For our setup we selected a balanced power supply. Another option is to use 9V batteries to provide a stable low noise input power to the load cell. However, batteries drain and in the case of a longer testing session the drained battery will cause an offset in the output voltages from the load cell.



Figure 16 - Load cell power supply

III.4 Data Acquisition

The project design requirements require from the DAQ system a very high sampling rate and comparably long sampling time. Many challenges have been overcome to meet those requirements. All of the hardware and software was provided to us by the Research Center at Natick. Fig. 17 below shows a graphical representation of the different links in the signal acquisition system.

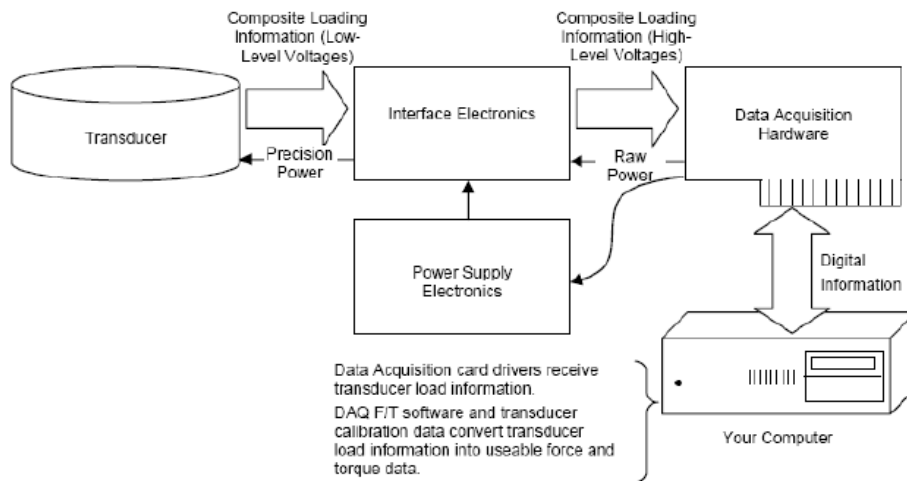


Figure 17: DAQ System Setup

High frequency of sampling combined with a long sampling period causes a major hardware and software malfunction expressed in buffer overflow of the DAQ PCI board. This was solved using an alternative, custom made LabView VI design.

The VI was developed so that it acquires and records voltages from the six channels of the transducer at a rate of 10 kHz. Time stamp resolution also matches sampling Parameters frequency. The voltages are then plotted to an FFT diagram and on a voltage vs. time graph and outputted to a .csv file. The outputted data file consists of 7 columns – a time stamp and the six axes from the transducer.

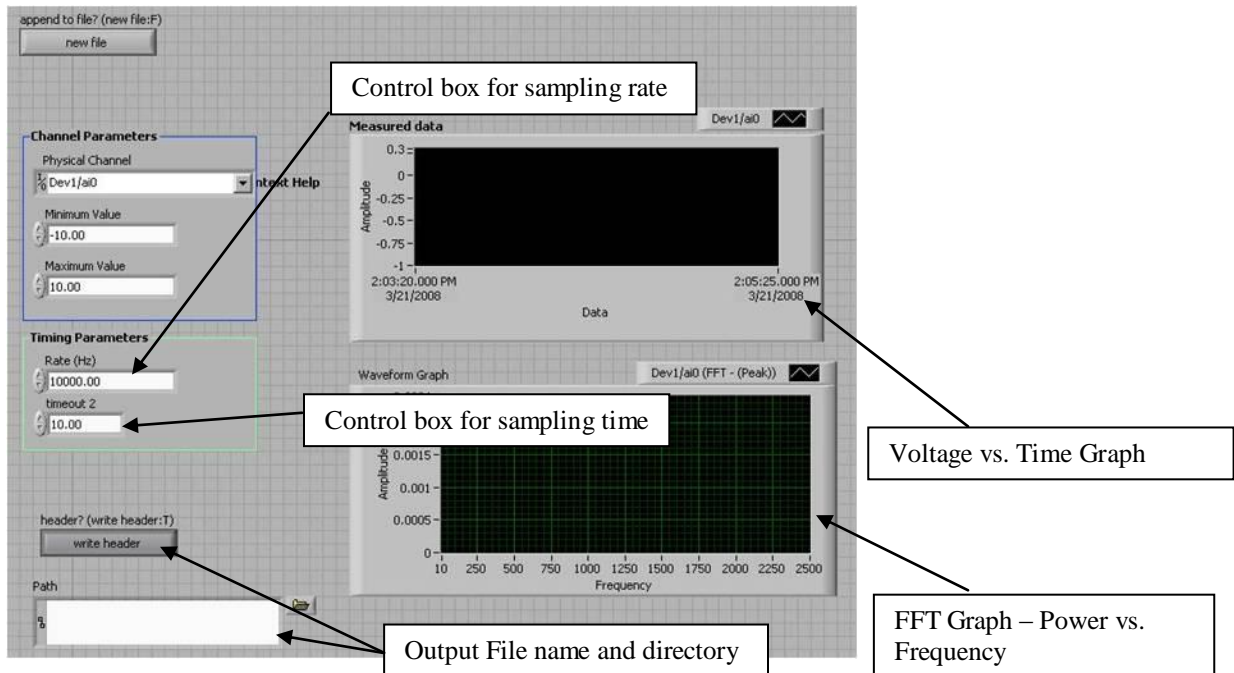


Figure 18 - LabView 8.2 VI

The block diagram shows our custom DAQ design capable of high frequency, long sampling time data acquisition and writing to an output file.

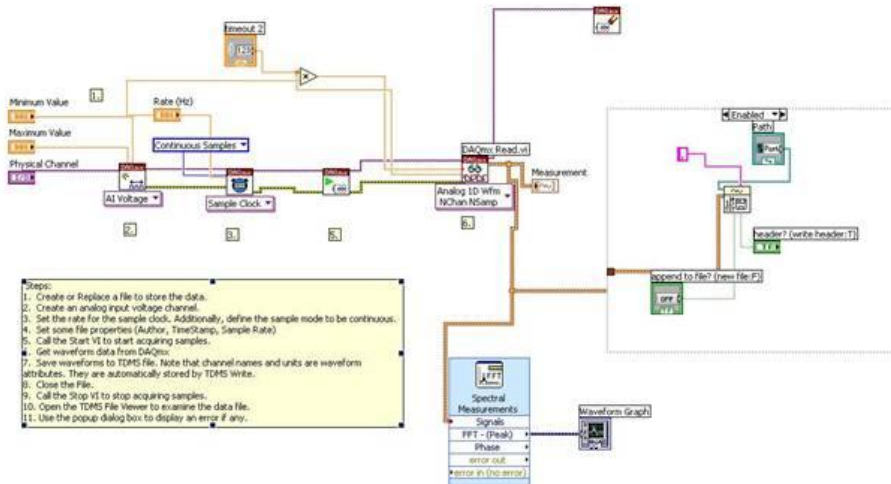


Figure 19 - Block Diagram

III.5 Final Design

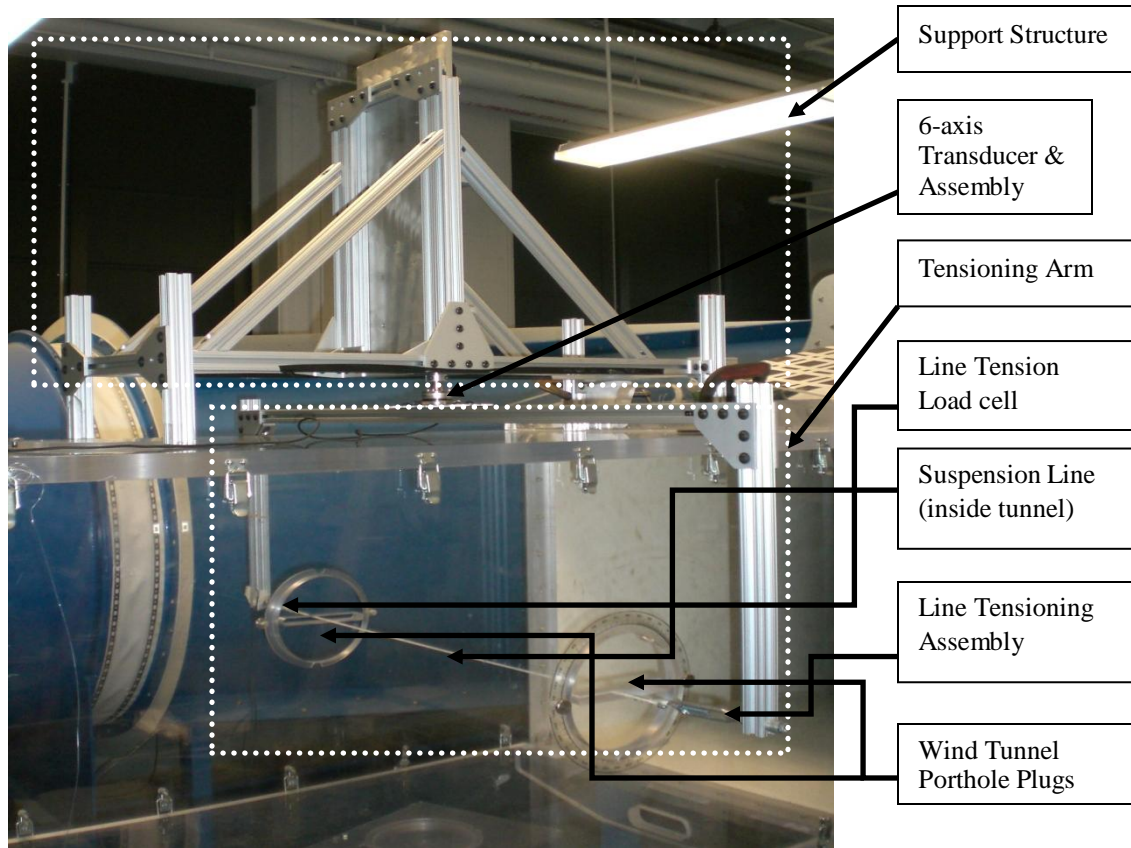


Figure 20: Final Structure Design

Figure 20 shows the final design manufactured designed and built. As shown in the above figure the entire structure is mounted on the wind tunnel and the tensioning arm hangs from the sensor. No alignment issues exist with this setup since all the aluminum extrusion arms slide to achieve perfect positioning. Simple tensioning mechanism and capability for a wide range of loads are essential to this design and have been achieved with the developed setup.

III.6 Dimensional Analysis

The goal of our testing is to mimic the behavior of an actual suspension line; however we are limited to collecting data only in the wind tunnel. This constraint poses a need for dimensional analysis, an engineering technique used to reduce the number of relevant physical variables in a problem to a smaller number of non-dimensional parameters. Using this technique, we will be able to draw comparisons between our model in the wind tunnel and the actual prototype parachute, which will enable us to directly relate our data to the real world situation. In our case, the length of our model is not the same as an actual suspension line; however, we can adjust the tension in the line and the wind tunnel velocity if needed to achieve dynamic similarity.

III.6.1 Equivalent Resonant Frequency

While testing in the wind tunnel, it is important that the model line behaves the same as an actual line on the parachute. The natural resonant frequency of the line should be the same between model and prototype. We will break the resonant frequency equation down to a function of a number of dimensionless parameters. Dynamic similarity states that if all of these dimensionless parameters are the same between model and prototype, then the resonant frequency is also the same. The following analysis will take you step by step through this process.

Dimensional Analysis of resonance frequency equation:

$$f_r = f(T, w, d, f_s, V_\infty, \rho_f, \mu, L) \quad (1)$$

Where,

$$f_r = \text{Resonance frequency} \left[\frac{1}{t} \right], \quad T = \text{Tension} \left[\frac{mL}{t^2} \right], \quad w = \text{Linear density}, \left[\frac{m}{L} \right]$$

$$d = \text{Line diameter} [L], \quad f_s = \text{Vortex shedding frequency} \left[\frac{1}{t} \right], \quad V_\infty = \text{Fluid velocity}, \left[\frac{L}{t} \right]$$

$$\rho_f = \text{Fluid density} \left[\frac{m}{L^3} \right], \mu = \text{Fluid viscosity} \left[\frac{m}{Lt} \right], L = \text{line length}, [L]$$

N = number of parameters = 9

J = number of dimensions = 3

N – J = 6 pi groups

ρ_f , V_∞ and d cannot be combined to form a pi group. We can use these three parameters along with other parameters to determine non-dimensional pi groups.

Group 1:

$$f_r \rho_f V_\infty d : \left[\frac{1}{t} \right] \left[\frac{m}{L^3} \right] \left[\frac{L}{t} \right] [L]$$

Combining these variables into a non-dimensional pi group: $\Pi_1 = \left[\frac{f_r d}{V_\infty} \right]$. This

represents the ratio between the velocity of the vibrating line compared to the velocity of the passing fluid.

Group 2:

$$T \rho_f V_\infty d : \left[\frac{mL}{t^2} \right] \left[\frac{m}{L^3} \right] \left[\frac{L}{t} \right] [L]$$

The pi group is: $\Pi_2 = \left[\frac{T}{\rho_f V_\infty d^2} \right]$. This represents the ration between the force

on the line due to tension compared to the force on it from the fluid.

Group 3:

$$w \rho_f V_\infty d : \left[\frac{m}{L} \right] \left[\frac{m}{L^3} \right] \left[\frac{L}{t} \right] [L]$$

The pi group is: $\Pi_3 = \left[\frac{w}{\rho_f d^2} \right]$. This represents the ratio of the amount of mass per length of the physical line versus the amount from the fluid.

Group 4:

$$F_s \rho_f V_\infty d : \left[\frac{1}{t} \right] \left[\frac{m}{L^3} \right] \left[\frac{L}{t} \right] [L]$$

The pi group is: $\Pi_4 = \left[\frac{f_s d}{V_\infty} \right]$. This is the Strouhal number, S. The Strouhal Number represents a measure of the ratio of inertial forces due to the unsteadiness of the flow or local acceleration to the inertial forces due to changes in velocity from one point to another in the flow field.

Group 5:

$$L \rho_f V_\infty d : [L] \left[\frac{m}{L^3} \right] \left[\frac{L}{t} \right] [L]$$

This simply forms a group: $\Pi_5 = \left[\frac{L}{d} \right]$, which is the aspect ratio (A) of the line.

Group 6:

$$\mu \rho_f V_\infty d : \left[\frac{m}{Lt} \right] \left[\frac{m}{L^3} \right] \left[\frac{L}{t} \right] [L]$$

The pi group formed is: $\Pi_6 = \left[\frac{\rho_f V_\infty d}{\mu} \right]$, the Reynolds number

Solving for the resonance frequency with respect to the 6 pi groups:

$$f_r = \left(\frac{V_\infty}{d} \right) g \left(\left[\frac{T}{\rho_f V_\infty d^2} \right], \left[\frac{w}{\rho_f d^2} \right], \left[\frac{f_s d}{V_\infty} \right], \left[\frac{L}{d} \right], \left[\frac{\rho_f V_\infty d}{\mu} \right] \right) \quad (2)$$

As long as the ratios from each pi group are the same between the model and the actual parachute, dynamic similarity will be achieved. If we test under conditions of dynamic similarity we can assume our results will be the same as those of real conditions.

Under testing conditions, our length is limited to 2 feet. Pi group number 5 (aspect ratio) will not be the same between model and prototype because we are using the same lines and therefore cannot change diameter to make up for the change in length. By combining two pi groups into one we can solve this problem.

Dividing group 2 by group 5 squared gives:

$$\frac{\left[\frac{T}{\rho_f V_\infty d^2} \right]}{\left[\frac{L}{d} \right]^2} = \left[\frac{T}{\rho_f V_\infty L^2} \right]$$

The resonance frequency with respect to the pi groups is now:

$$f_r = \left(\frac{V_\infty}{d} \right) g \left(\left[\frac{T}{\rho_f V_\infty L^2} \right], \left[\frac{w}{\rho_f d^2} \right], \left[\frac{f_s d}{V_\infty} \right], \left[\frac{\rho_f V_\infty d}{\mu} \right] \right) \quad (3)$$

Once again, the only parameter that differs between model and prototype is L, so $\left[\frac{T}{\rho_f V_\infty L^2} \right]$ is the only pi group that needs attention. This ratio must be equal between model and prototype in order to achieve dynamic similarity.

Solving for our model tension:

$$\left[\frac{T_m}{\rho_f V_\infty L_m^2} \right] = \left[\frac{T_p}{\rho_f V_\infty L_p^2} \right] \Rightarrow T_m = \frac{T_p L_m^2}{L_p^2} \quad (4)$$

This equation will be used to determine the tension we will apply in the wind tunnel. Having achieved dynamic similarity, the resonant frequency between model and prototype will be the same.

III.6.2 MC-4 Prototype Specifications

By examining the MC-4 Parachute Assembly schematic (Drawing No. 11-1-3518), one can determine the actual line lengths (L_p) of the parachute. By using the maximum specified suspended weight for the MC-4 of 360 lbs, one can also estimate the tensions (T_p) in the lines of the parachute during free flight.

Sixteen main lines branch off of the paratrooper. These lines have lengths of 11' and 9'3". Each line supports 22.5 lbs assuming each line carries an equal load.

Then, each of these sixteen lines split creating a total of 32 lines. These lines have lengths of 14'6", 14'9", 66", and 54". Each line supports 11.25 lbs assuming each line carries an equal load.

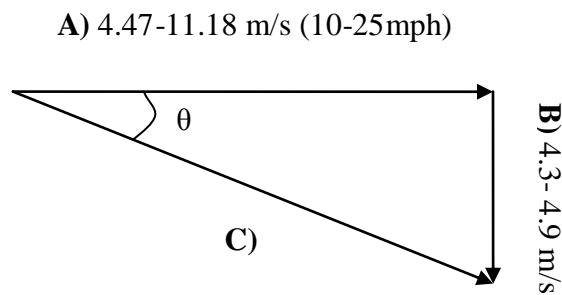
There are six different relations between L_p and T_p . Solving for T_m from equation (4) above:

$\underline{L_p}$	$\underline{T_p}$ (lbs)	$\underline{T_m}$ (lbs)
11'	22.5	.744
9'3"	22.5	1.052
14'6"	11.25	.214
14'9"	11.25	.207
66"	11.25	1.488
54"	11.25	2.222

By tensioning the model line in the wind tunnel to these tensions, conditions will be properly matched between the model and the actual parachute. Also keep in mind that these are independent of wind tunnel air velocity, which must be set to an appropriate airspeed for an operating parachute.

Looking at the horizontal and vertical velocity ranges for the MC-4 parachute from its technical specifications:

Operating velocity ranges for MC-4:



A) – Horizontal velocity range

B) - ROD (Rate of decent)/Vertical velocity range

C) – Flight vector

$$C = \sqrt{B^2 + A^2} = 6.2 - 12.21 \frac{m}{s}$$

$$\theta = \text{Arc tan}\left(\frac{B}{A}\right) = 21 - 42.4^\circ$$

Using the actual velocity ranges of the MC-4 parachute and the model line tensions as calculated before, the group came up with an experimental matrix of tests to run with the MC-4 suspension lines. This can be seen in Appendix I.

III.6.3 Vortex Shedding

One important case to look at would be when the vortex shedding frequency of the line equals the natural resonant frequency. In this case, the line would vibrate with

large amplitude and it would be interesting to see how this affects drag. First let me lay out some properties of the MC-4 suspension line as measured by the group:

Line Dimensions (wind tunnel test section)	0.1" x 0.3" x 2'
Approximate Diameter (based on area):	0.195"
Linear Density, w	.225 lb/ft

Table 1: MC-4 Suspension Line Properties

The resonance frequency of a line oscillating solely due to tension in a vacuum is:

$$f_r = \frac{1}{2L} \sqrt{\frac{T}{w}} \quad (5)$$

The resonance frequency is shown in Fig. 18 for the MC-4 suspension line:

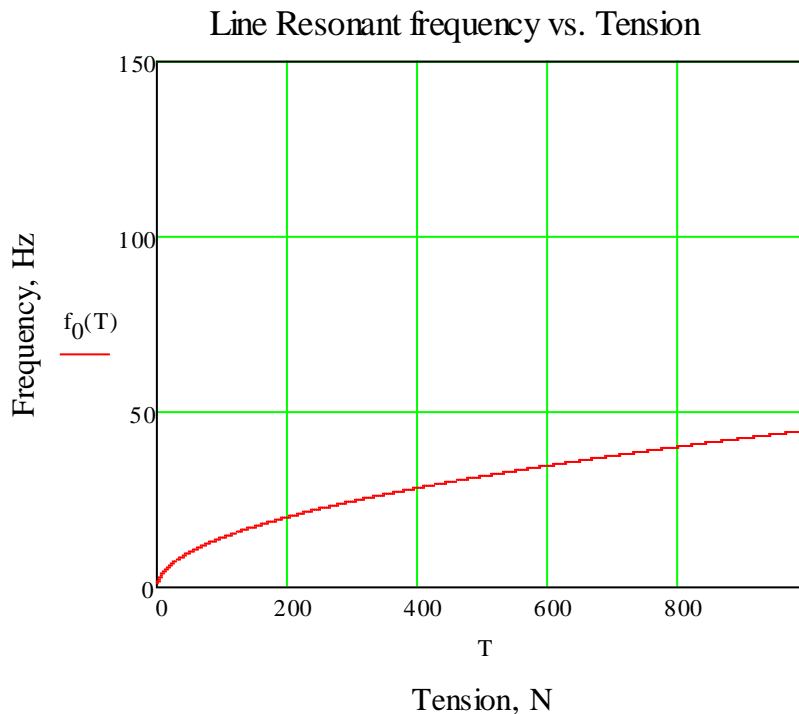


Figure 21 - Line Resonant Frequency vs. Tension

Based on experimental testing, the Strouhal number (based on vortex shedding frequency) for a smooth cylinder is (7):

$$S = \left[\frac{f_s d}{V_\infty} \right] \cong .18 \quad (6)$$

Solving for f_s : $f_s = \frac{.18V_\infty}{d}$

This can also be represented graphically using the MC-4 suspension line properties:

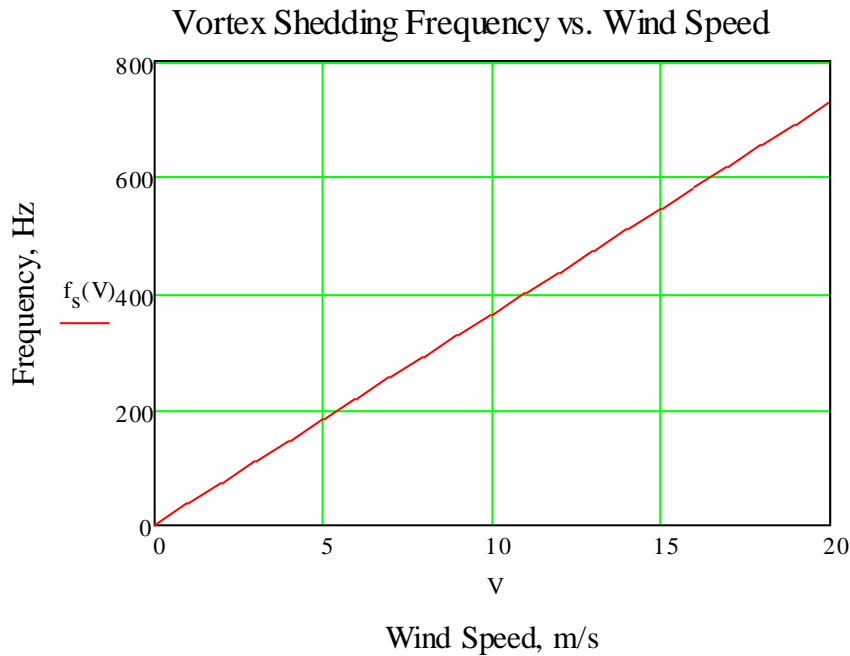


Figure 22 - Vortex Shedding Frequency vs. Wind Speed

Setting f_s equal to f_r and solving for T :

$$\frac{1}{2L} \sqrt{\frac{T}{w}} = \frac{.18V_\infty}{d} \Rightarrow T = \left(\frac{.36LV_\infty}{d} \right)^2 w \quad (7)$$

Solving for tension with respect to velocity, using MC-4 suspension line properties in metric units:

$$T = \frac{657.7V^2 \cdot \text{kg}}{\text{m}} \quad (8)$$

Plotting these results, again using the properties of the MC-4 suspension lines:

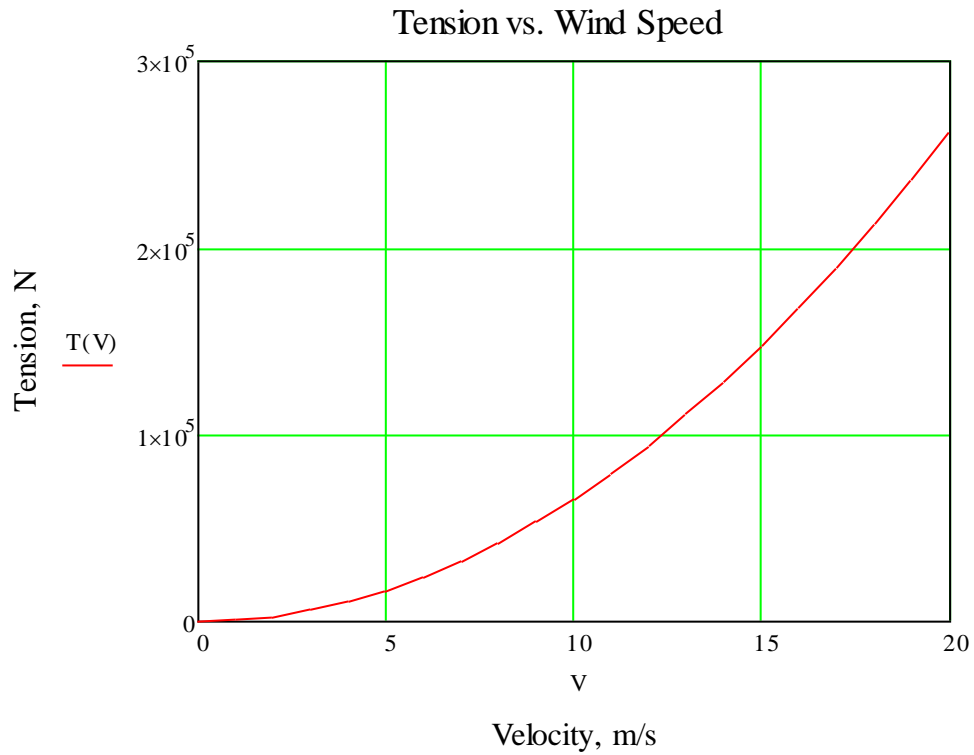


Figure 23 - Tension vs. Wind Speed

With the current setup, tensions of this magnitude are unachievable. With a free stream velocity of 10 m/s, the MC-4 line would need to be tensioned to approximately 670 kilograms in order to match the resonant and vortex shedding frequencies.

III.7 Calculations

Before running any experiments, it was important to determine the magnitude of the suspension line drag we would expect to measure. For this purpose we assumed the line to be a smooth circular cylinder. Using properties of atmospheric air, Reynolds number curves were plotted for various line diameters and wind speeds based upon the Reynolds number equation:

$$\text{Re}(d) := \rho \cdot V \cdot \frac{d}{\mu}$$

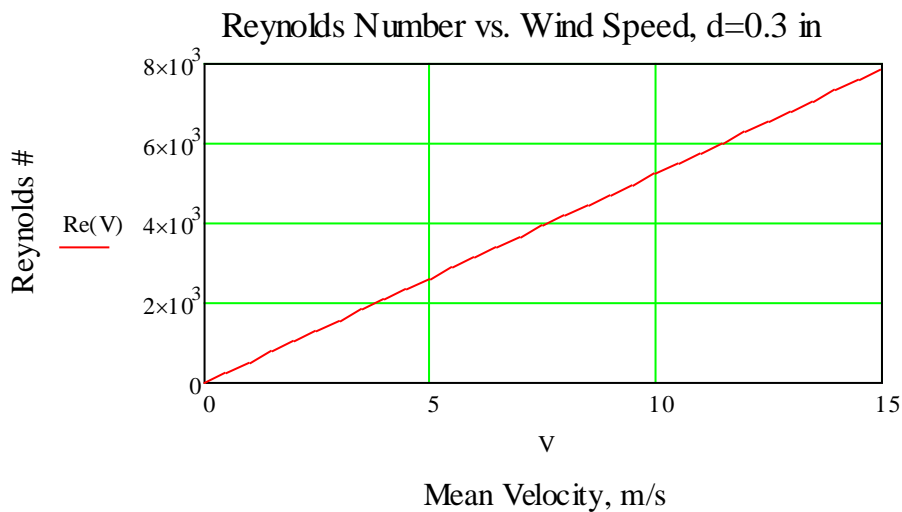


Figure 24 - Re vs. Wind Speed

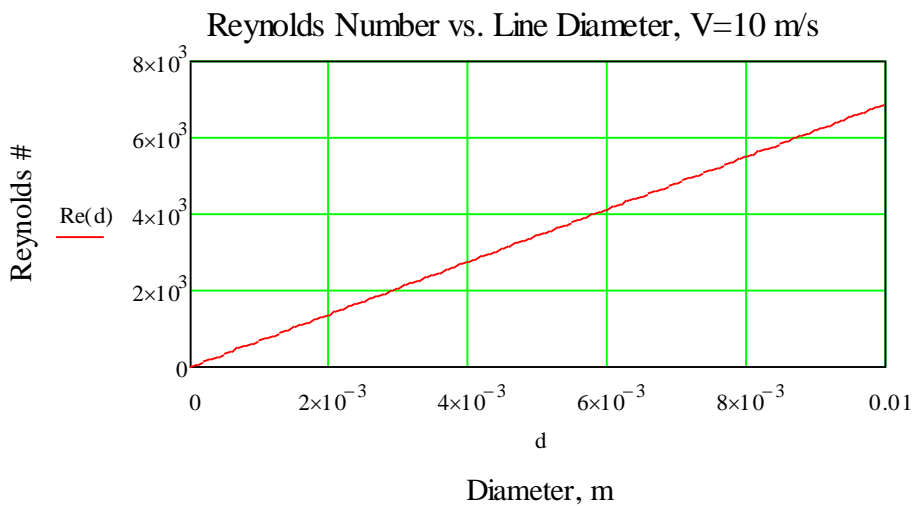


Figure 25 - Re vs. Line Diameter, $V=10$ m/s

For the range of Reynolds numbers that the suspension lines will see, the drag coefficient is near a value of 1, as seen in Figure 24 (7).

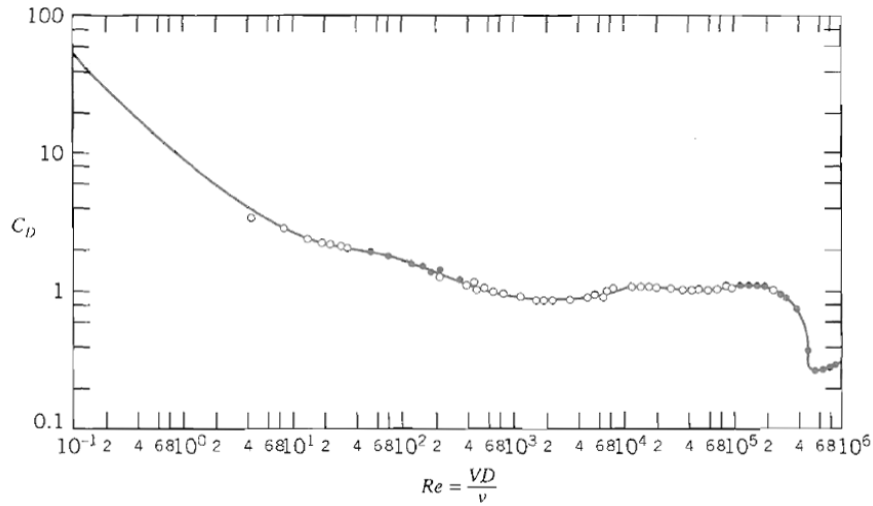


Figure 26 - Drag Coefficient vs. Re (9)

Knowing the drag coefficient and size of the wind tunnel, graphs of the expected line drag were also made:

$$C_d := 1$$

$$l := 2\text{ft}$$

$$D(d) := d \cdot l \cdot C_d \cdot 0.5 \cdot \rho \cdot V^2$$

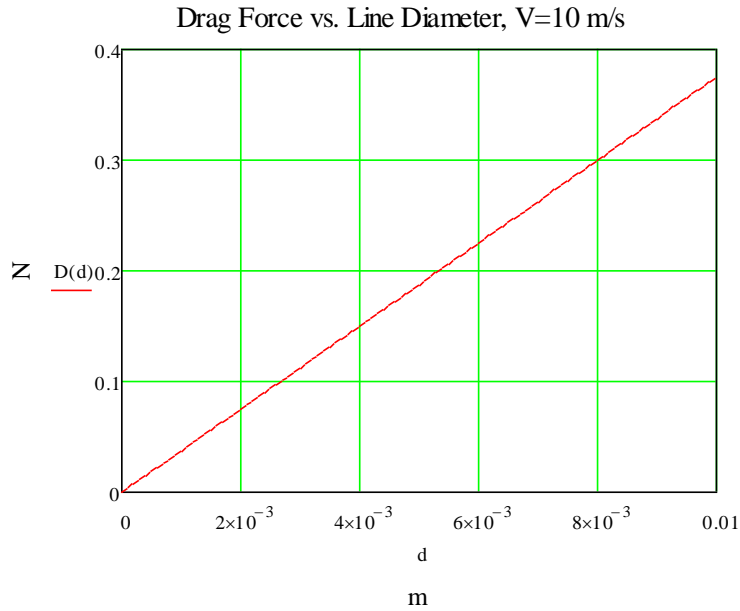


Figure 27 - Drag Force vs. Line Diameter, V=10m/s

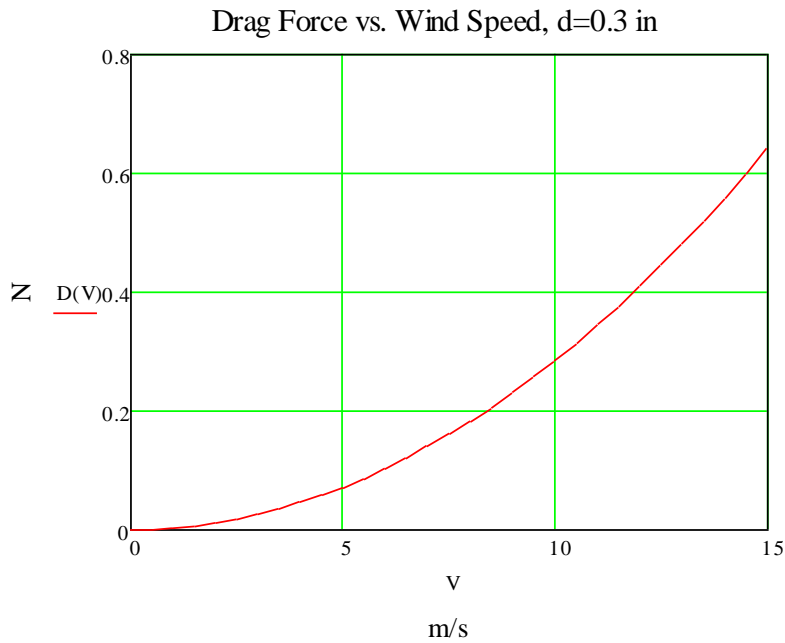


Figure 28 - Drag force vs. Wind Speed, d=0.3 m

Due to the short, 2 foot section of wind tunnel and the relatively small diameters of the lines, we can expect to observe drag forces on the lines, in the range of 0-0.6 N, or 0-60 grams. These drag forces are within the resolution range ($\pm 1/900 \text{ N} = \pm 1 \text{ gram}$) of the force transducer used in the study. However, drag values in this range (0-60 g) are

still difficult to measure in experiments, especially due to noise associated with vibrations from the wind tunnel.

This force range may be well within the resolution of the six-axis transducer but the disturbances from all the external components which are part of the entire setup add to the noise – to signal ration making it extremely hard to analyze and to extract useful data.

IV. Testing Methodology

Although slight alterations were made throughout the completion of the project, a basic methodology was used for each testing segment. The testing was broken up into five basic steps: construction, electronic setup, bias testing, drag testing, and data extraction. The following sections constitute a ‘user’s manual’ for others to investigate who would wish to repeat the experiments.

IV.2 DAQ Equipment Setup

The DAQ system set up was a relatively simple procedure once our computer was based by the wind tunnel. In order to acquire voltage signals from the six axis transducer it has to be connected to an Interface Electronics Unit and to a power supply which are all part of the transducer setup. The high voltage signal is then sent to the PCI DAQ Card in the computer which has LabView 8.2 installed (see App. D).

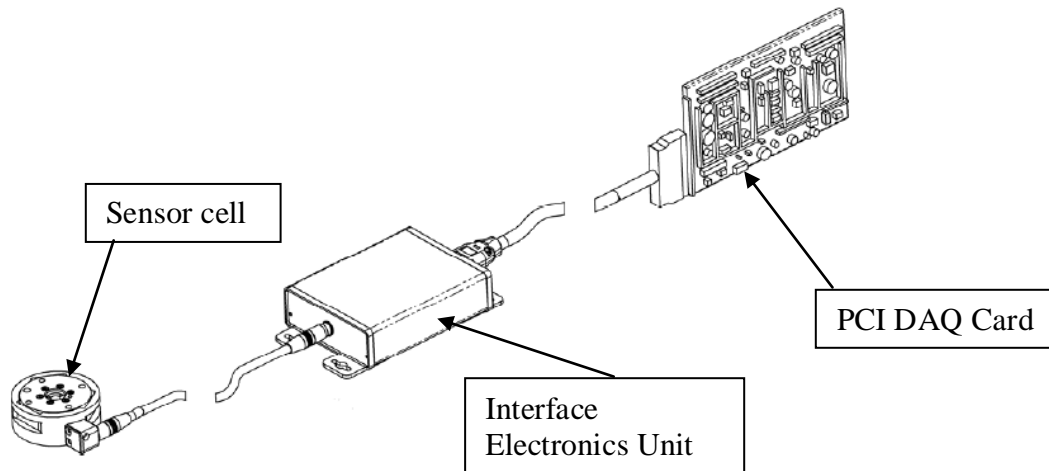


Figure 29 – DAQ Connection diagram

Even though we are interested in only two of the sensing axes of the transducer to obtain drag data, all the axes output voltages are being recorded. This is done so we could investigate any unpredicted phenomenon created by the line being in the free stream flow. If no disturbances occur the bias taken before hand will annul the DC offset in any when the data files are run through the MATLAB analysis code.

After the sensor is setup and connected to the PC equipped with DAQ PCI onboard card and the LabView Visual instrumentation is configured, the alignment

procedure can begin. Using ATI DAQ F/T Bias Software tool (note: the ATI DAQ software cannot be used simultaneously with LabView) all the six axes can be aligned so no force or weight components exist (Fig 30). The ATI software is examined to ensure there are no forces except for the weight of the arm in the z-direction. If this is not the case the tensioning arm positioning can be adjusted removing any moments created by an offset of center of gravity.

At this point ATI software provided by our liaison is opened on the computer and the forces are biased out. The user interface can be seen below. This establishes a starting point for alignment purposes throughout the rest of the setup.

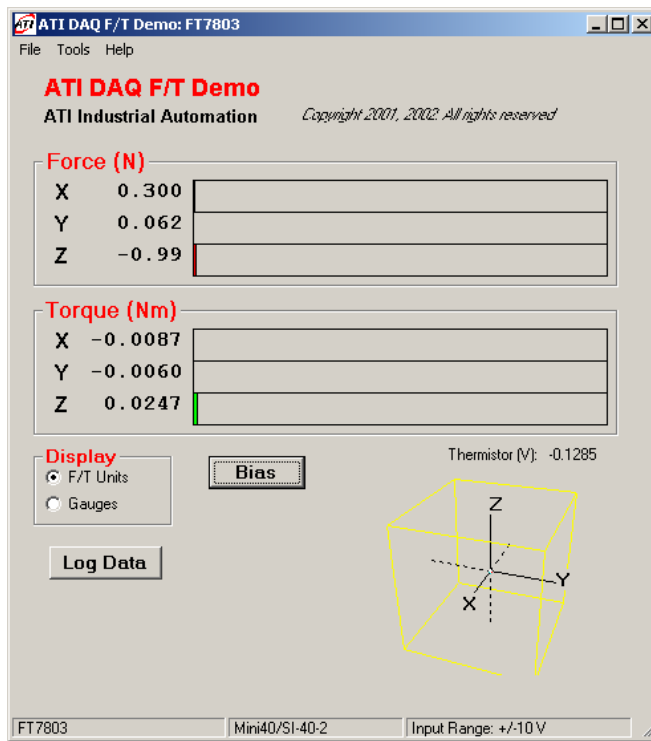


Figure 30: ATI DAQ F/T Demo Software User Interface

IV.1 Apparatus Setup

The constructed base apparatus should be assembled on top of the wind tunnel in the following manner. The support structure of the apparatus should be placed in a position parallel to the top of the wind tunnel. The apparatus is tightly clamped to the edge so only the movement of the line being tested is recorded; the motion of the

apparatus would be the same as that of the wind tunnel. Excellent horizontal plane alignment can be achieved because of the adjustability of each of the four legs of the support structure. As Fig. 26 shows perfect alignment to the horizontal is possible.

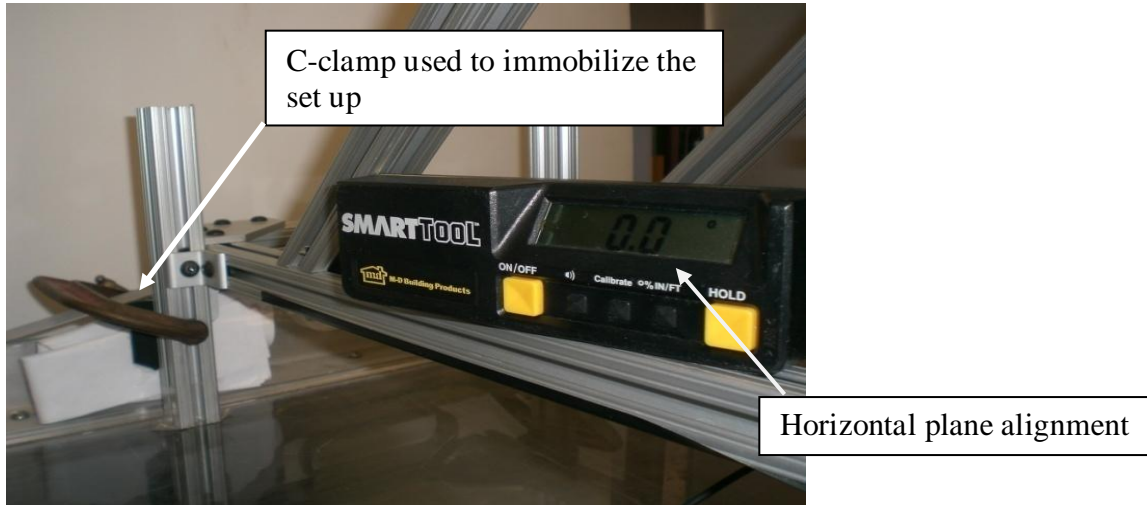


Figure 31 - Support structure alignment

We have developed a procedure for building the set up since it has to be taken on and off the wind tunnel on a regular basis. This procedure allowed us to easily reassemble the apparatus with minimal initial misalignment. First, we attach the transducer to the circular mount using three #2-40 screws spaced at 120 deg. Next, the back plate is attached to the circular mount with the sensor. Having this configuration makes it easy to handle and attach to the support structure later on.



Figure 32: Circular Mount Attached to the Back Plate

The tensioning arm is then attached to the transducer section (Fig 33). A stack of paper is placed between the tensioning arm and wind tunnel test section in order to align this connection. The paper stack also supports the weight of the arm during bolting to ensure that no excessive forces/moments are placed on the transducer. Once the arm is aligned evenly and screwed into the base apparatus, the paper is removed.

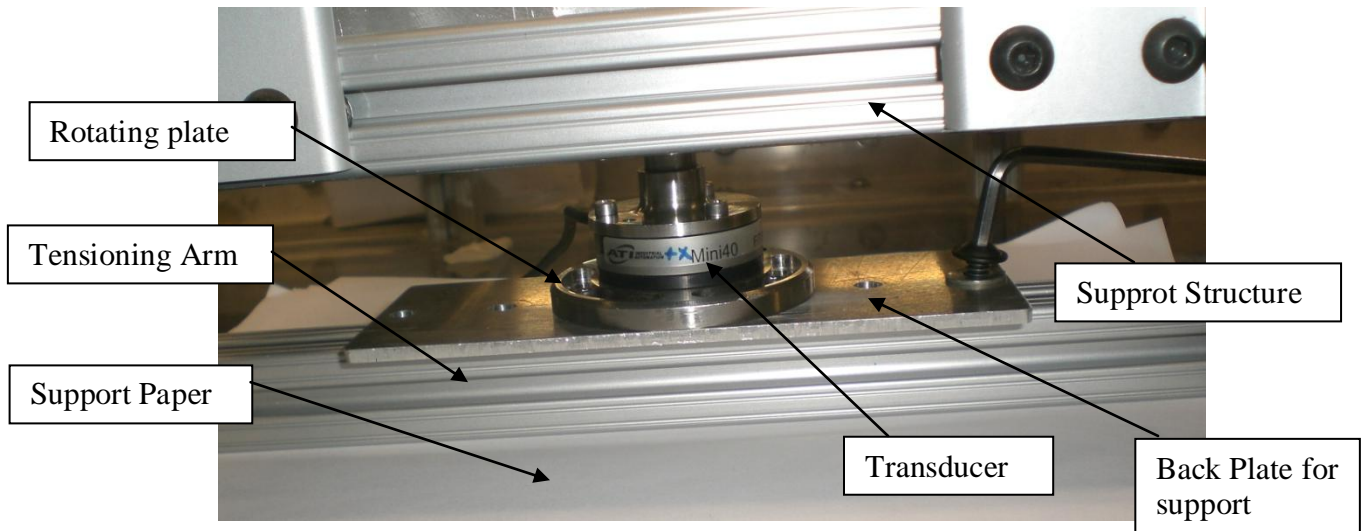


Figure 33 - Last assembly step

Once the entire setup is in place and the DAQ system functioning, we use the DAQ F/T tool to verify the alignment. The only force/moment component present should be the Z axis representing the weight of the tensioning arm. Bias data collection can be initiated after this step.

IV.3 Bias Testing

The offset of voltage output from the six axis transducer is comparable to the drag induced voltages resulting in incorrect combined output. To remove this DC offset a bias file is created before each measurement set and later used to subtract it from the measurements data files. The bias is taken as a test file having the same length and sampling frequency as the intended test files so that the format is kept the same avoiding any discrepancies. The bias is basically a measurement test with the tensioning arm attached to the supporting structure but no line. A new bias has to be created for each wind speed to account for the vibrations of the wind tunnel itself. The bias files then are used as an input to the MATLAB code discussed in Drag Testing below to remove the DC offset.

IV.4 Drag Testing

Once the entire set up has been constructed and aligned, the actual data extraction can begin. Fig 31 shows the path the voltage readings take to be interpreted as clean force and moment readouts.

There are several steps that need to be taken before the closed circuit wind tunnel can be used. Power switch is first, followed by connecting an air pressure hose and letting the cool water circulate through the heat exchanger. The external control panel allows accurate flow velocity adjustment.

After having the right tension on the line, the entire setup is positioned and aligned and the right free stream speed has been achieved data recording can begin. This is done by letting the LabView VI to run for 100s (program has a self timer) and to record the data to a .csv file. This step represents the first arrow in Fig 34.

IV.5 Data Extraction

After drag testing has been completed, the data needs to be run through two MATLAB codes before useful mean drag values can be seen. This process is illustrated in Fig. 31.

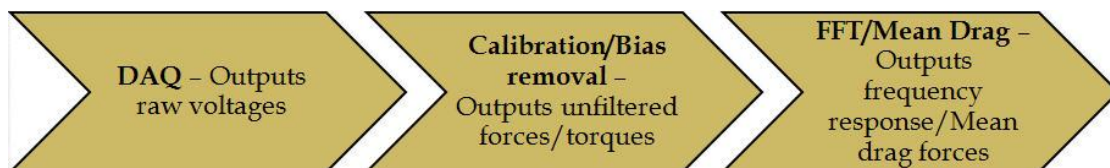


Figure 34 - From raw voltages to filtered forces and torques

First, raw voltage data is acquired from the six axes of the sensor. Sampling at 5,000 hertz over 100 seconds results in 500,000 data points for each axis. Using MATLAB codes seen in Appendices M and N, the raw data is then matched against the bias data

and calibration curves from the sensor's last calibration (July, 2007). The output of this code is force and torque data for each of the six axes; again, 500,000 points each.

This data was shown to be quite noisy, so further analysis was done. The last step in data extraction involved another MATLAB code, seen in Appendix O. This code was used to extract mean drag and also perform Fast-Fourier Transform on the data.

V. Results and Analysis

Analysis of the wind tunnel data proved to be quite cumbersome. High noise due to vibration was seen early in the project; however no absolute solution to this problem was produced. Fast Fourier Transform was able to show the frequency response of the data, but once again no ‘all-encompassing’ filter was able to be built to clean the data.

A typical signal over a one hundred second period can be seen below. Long, sine-like waves can be seen over periods of about 10 seconds. Also note the amplitude of the signal; greater than 15 Newtons. The noise is orders of magnitude higher than the expected drag, 0.1-0.2 N.

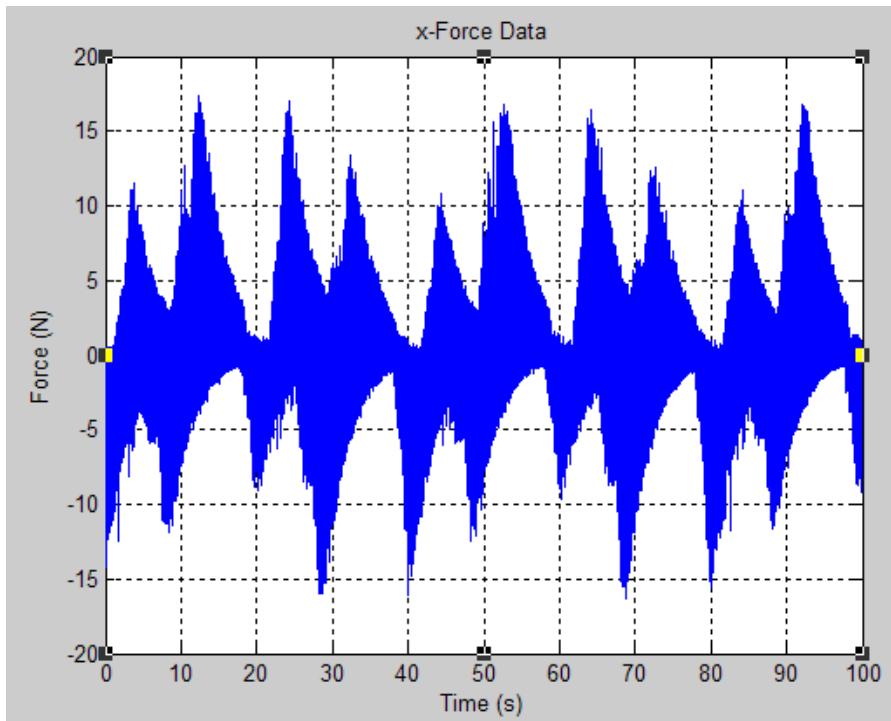


Figure 35: Raw drag data: Low frequency noise

The raw drag signal also contained very high frequency noise. Figure 33 shows the signal in a range of .25 seconds.

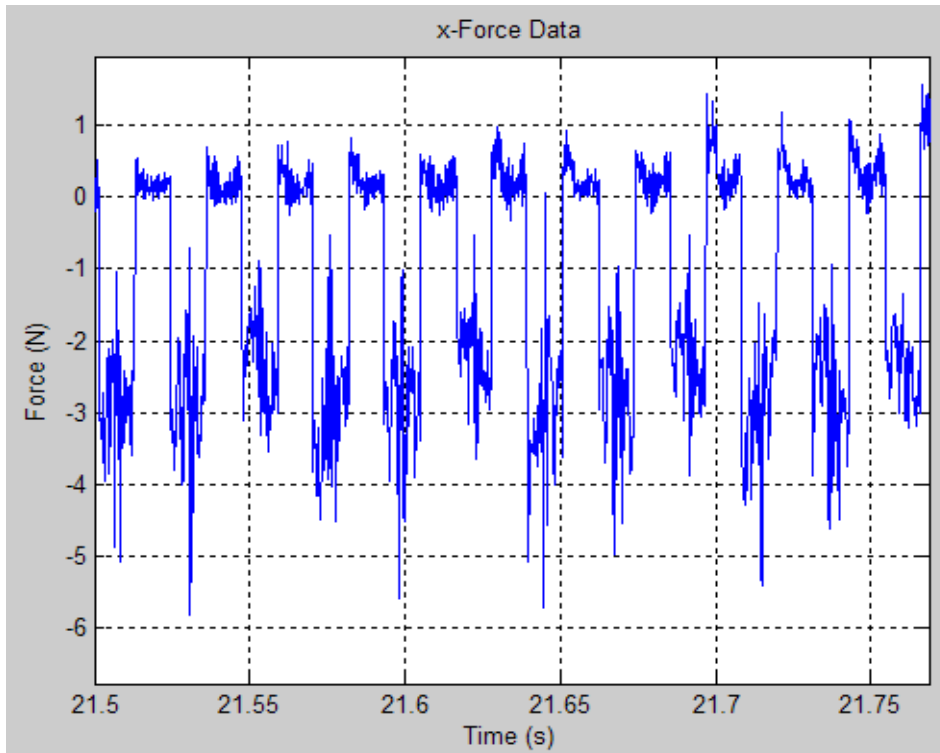


Figure 36: Raw drag data: High frequency noise

Fast Fourier analysis proved this distinction of low and high frequency noise response. For all tests conducted, there were two distinct spikes in the FFT, as seen in Fig. 35. The first, corresponding to the low frequency noise, was at around .1 hertz for all data collected (Fig. 36). The second spike, resulting from vibrations in the wind tunnel, occurred anywhere from 40-90 hertz, depending on the speed of the wind tunnel (Fig. 37). Higher frequency spikes seen are harmonics of the first vibration spike.

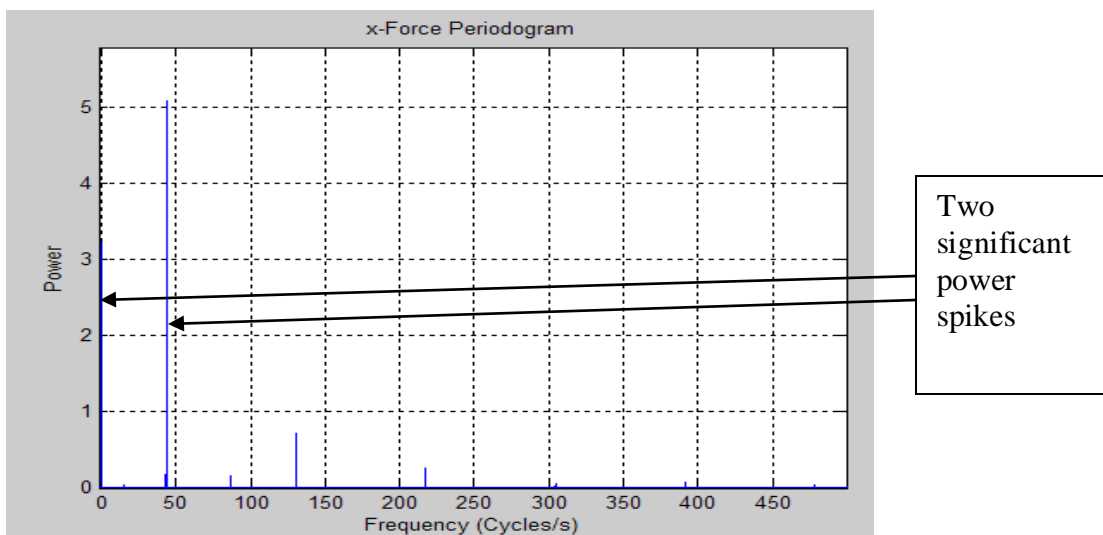


Figure 37: Drag data FFT

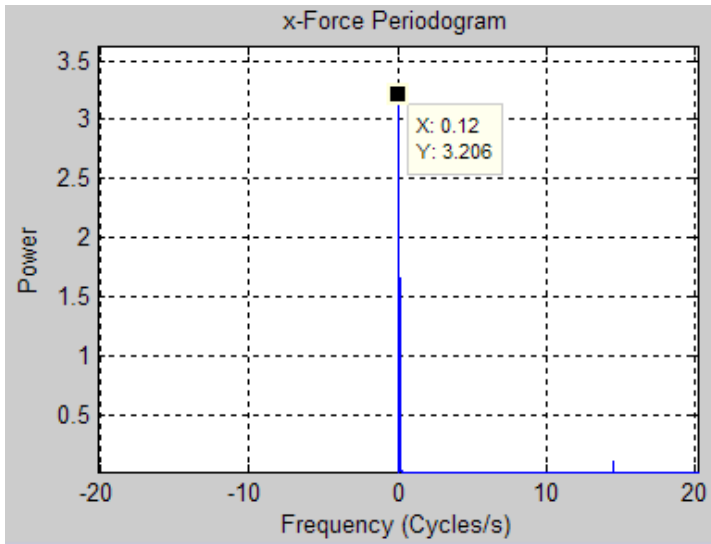


Figure 38: FFT for Low Frequency Response

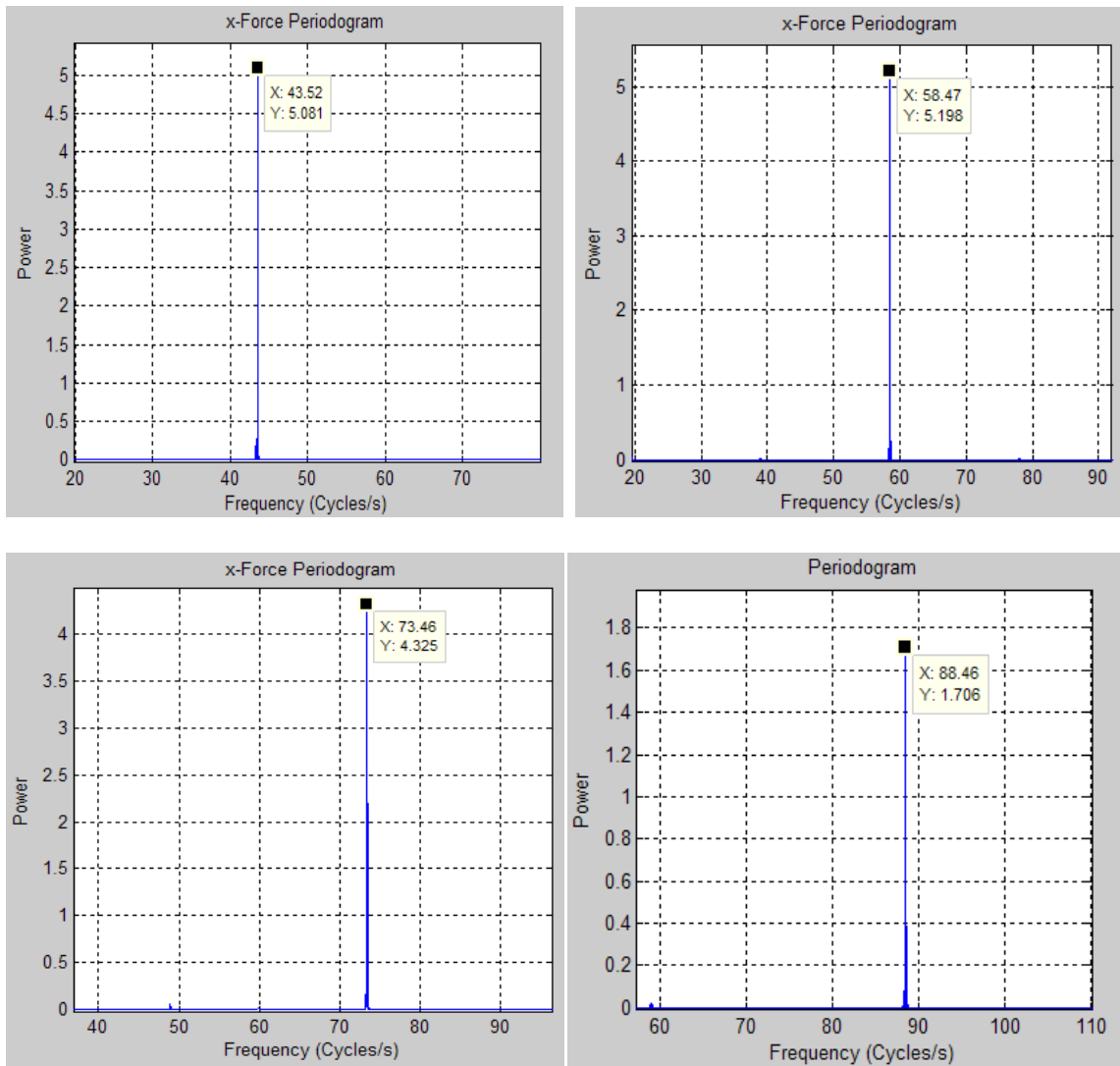


Figure 39: Vibration Frequency Response for Windspeeds 6, 8, 10, and 12 m/s

The final experiments that were run are those shown highlighted in Appendix I. The mean drag data from those experiments can be seen in Appendix J. The mean drag data collected is not perfectly consistent; there are variations of close to .2 N between runs at the same wind speed and line orientation.

However, obvious trends can be seen which validate our collection procedures. In examining the data overall, as wind speed increases, drag increases. Furthermore, as line diameter increases drag increases. Seeing these expected trends shows that valid data could be extracted with more work.

Another interesting note is that as a whole the drag of the collected data was higher than had been approximated in earlier calculations. For a smooth cylinder with a 0.3 inch diameter and wind speed of 10 m/s, we calculated a drag of 0.3 N. The perpendicular orientation of the MC-4 suspension line has an area normal to the flow of 0.3 inches as well, but at 10 m/s we measured a drag of 1.105 N. The source of this discrepancy can be due to a number of factors. First of all, the line is not a cylinder; it is more of a plate. The line is flexible in nature, while we were calculating for a solid cylinder. Lastly, the stitching of the line creates an obvious surface roughness which could affect the drag.

VI. Conclusions

Throughout the span of the project we have strived to obtain accurate and reliable results which would help examine the aerodynamic drag on suspension lines. Many obstacles have come in our way and most of which related to the high signal to noise ratio we obtain from drag testing. These issues arise from the small drag forces created from the lines and the comparably high noise induced from the vibrating wind tunnel and other electrical sources. MATLAB tools have been developed to examine and understand the output data so that more reliable results are obtained. This includes, Fast Fourier Transforms and filtering techniques.

The test structure and the entire DAQ setup have been designed for minimum weight and maximum durability. Bending moments from tensioning the line causes insignificant bending on the tensioning arm in the apparatus thus providing no threat to the transducer or any other part of the assembly. The DAQ equipment and software is

capable of high frequency data acquisition and long sampling time enabling the FFT analysis to capture low and very high frequency noise patterns.

However, we were unable to conduct all the experiments entries in our experimental matrix. This lack of sufficient data points in our analysis makes it hard to arrive at any solid conclusions of distinct line drag behavior.

To conclude, the constructed apparatus and the DAQ system developed for this project proved to be reliable, easy to assemble, extremely cost effective and with great features. Powerful software tools have been developed as well. However more in depth signal analysis together with bigger data volume should be done to arrive at any conclusive results.

VII. Recommendations

The goal of this project was to analyze aerodynamic drag on parachute suspension lines. An experimental apparatus was constructed together with a sophisticated data acquisition system to investigate possible drag causing phenomenon. Several key points regarding future work and recommendations have to be made.

Stemming from our dimensional analysis a test matrix was constructed to explore different real world situations in which the test specimen can be found. However, the majority of the experiments have been left as future work because of time constraint. Running the entire test matrix will ensure a broad spectrum of data that would cover a wide variety of phenomena that can be correlated to line drag.

As stated before we have encountered many problems with the high noise – to – signal ration in our measurements. Using the currently developed structural support and overall DAQ setup few improvements can be made to achieve lower noise values in comparison to output signal. Various alternatives can be employed to target the noise issues which result from the resonating closed circuit wind tunnel. It is recommended, resulting from our investigation of the above mentioned issues, disconnecting the entire test structure from the wind tunnel would reduce the amount of vibrations significantly.

Furthermore, it is suggested that a better understanding of the output signals is acquired. Once significant amount of data have been obtained more in depth signal analysis should be pursued. We have developed sophisticated methods of analyzing the

entire frequency domain of the vibrating setup with the line in the free stream. A better filtering strategy should be developed geared towards cleaning the undesired noise in the signal. This would ensure cleaner data which will in turn provide higher confidence in deducting any conclusions from the results.

In conclusion, running the entire test matrix using a less noisy setup and a better understanding of the gathered results is enough to obtain high confidence experimental results.

References

1. **Ikenson, Ben.** *Patents, Ingenious Inventions: How They Work and How They Came to Be.* New York : Black Dog and Leventhal Publishers, 2004.
2. **Command, U.S. Army Soldier & Biological Chemical.** New Parachute System. *SBCCOM - Natick Press Release.* [Online] January 9, 2001.
<http://www.natick.army.mil/about/pao/2001/01-01.htm>.
3. **U.S. Army Research, Development and Engineering Command.** About Natick Soldier RD&E Center (NSRDEC). *NSRDEC: U.S. Army Natick Soldier Research, Development and Engineering Center.* [Online]
<http://nsrdec.natick.army.mil/about/index.htm>.
4. —. Warfighter Protection & Aerial Delivery Directorate (WarPAD2): Airdrop / Aerial Delivery. *NSRDEC: U.S. Army Natick Soldier Research, Development and Engineering Center.* [Online] <http://nsrdec.natick.army.mil/about/airdrop/index.htm>.
5. **Desabrais, Kenneth.** Project Meeting. Worcester, MA, USA : s.n., September 2007.
6. **Lingard, Steve.** *H.G. Heinrich Parachute Systems Short Course.* Yuma, AZ : U.S. Army Proving Ground, 2004.
7. MC-4 Ram Air Parachute System. *Strong Enterprises: The parachute company with imagination.* [Online] 2006.
http://www.strongparachutes.com/Pages/mil_MC4_Mission_chute.htm.
8. **Futek.** Miniature S Beam Load Cell. *Futek Company Web Site.* [Online]
<http://www.futek.com/product.aspx?stock=FSH00098&acc2=accl>.
9. **Robert W. Fox, Alan T. McDonald, Philip J. Pritchard.** *Fluid Mechanics.* s.l. : John Wiley & Sons Inc; 6International Ed edition, 2006.
10. *Para-Flite.* [Online] Para-Flite. www.airbornesystems-na.com.

Appendices

Appendix A - S-Beam Junior Load Cell

FUTEK MODEL LSB200 (L2357)

Drawing Number: F11041

INCH [mm] | R.O.= Rated Output

WIRING CODE (WC1)

+Excitation	-Excitation	+Signal	-Signal
RED	BLACK	GREEN	WHITE

S-BEAM JUNIOR LOAD CELL

DESIGNED FOR INLINE LOADING IN TENSION & COMPRESSION

AVAILABLE IN #4-40 AND M3x0.5 METRIC THREADS

SPECIFICATIONS:

RATED OUTPUT	1.5 mV/V nom. (100 g), 2 mV/V nom. (250 g to 100 lb)
SAFE OVERLOAD	1000% of R.O. (100 g to 100 lb), 200% of R.O. Tension Only (50 lb and 100 lb)*
ZERO BALANCE	±3% of R.O.
EXCITATION (VDC OR VAC)	5 MIN, 10 MAX
BRIDGE RESISTANCE	350 Ω nom.
NONLINEARITY	±0.1% of R.O.
HYSTERESIS	±0.1% of R.O.
NONREPEATABILITY	±0.05% of R.O.
TEMP. SHIFT ZERO	±0.01% of R.O./°F [0.018% of R.O./°C]
TEMP. SHIFT SPAN	±0.02% of LOAD/°F [0.036% of LOAD/°C]
COMPENSATED TEMP.	60 to 160°F [15 to 72°C]
OPERATING TEMP.	-60 to 200°F [-50 to 93°C]
WEIGHT	0.3 oz [9 g] (100g to 10 lb), 0.9 oz [26 g] (25 to 100 lb)
DEFLECTION	0.002 [0.05] TO 0.005 [0.13]

CABLE: #29 AWG, 4 Conductor, Spiral Shielded Silicone Cable, 5 ft [1.5 m] Long

ACCESSORIES AND RELATED INSTRUMENTS AVAILABLE

CALIBRATION (STD) 5 pt TENSION; 60.4KΩ SHUNT CAL. VALUE (For 2 mV/V), 75KΩ SHUNT CAL. VALUE (For 1.5 mV/V)

CALIBRATION (AVAILABLE) COMPRESSION

CALIBRATION TEST EXCITATION 5 VDC

*SENSOR STRUCTURE CAN HANDLE HIGH OVERLOADS BUT #4-40 and M3x0.5 THREADS MAY LIMIT OVERLOAD AT HIGHER CAPACITY

Stock #	Capacity (lb)	Capacity (N)	Thread Size	Material
FSH00089	100g	1	#4-40	Aluminum
FSH00099			M3x0.5	
FSH00090	250g	2.5	#4-40	
FSH00100			M3x0.5	
FSH00091	1	4.5	#4-40	
FSH00101			M3x0.5	
FSH00092	2	8.9	#4-40	
FSH00102			M3x0.5	
FSH00093	5	22.2	#4-40	
FSH00103			M3x0.5	
FSH00095	10	44.5	#4-40	
FSH00104			M3x0.5	
FSH00096	25	111	#4-40	
FSH00105			M3x0.5	
FSH00097	50	222	#4-40	17.4ph S.S
FSH00106	100	445	M3x0.5	
FSH00098			#4-40	
FSH00107			M3x0.5	

FUTEK

ADVANCED SENSOR TECHNOLOGY, INC.

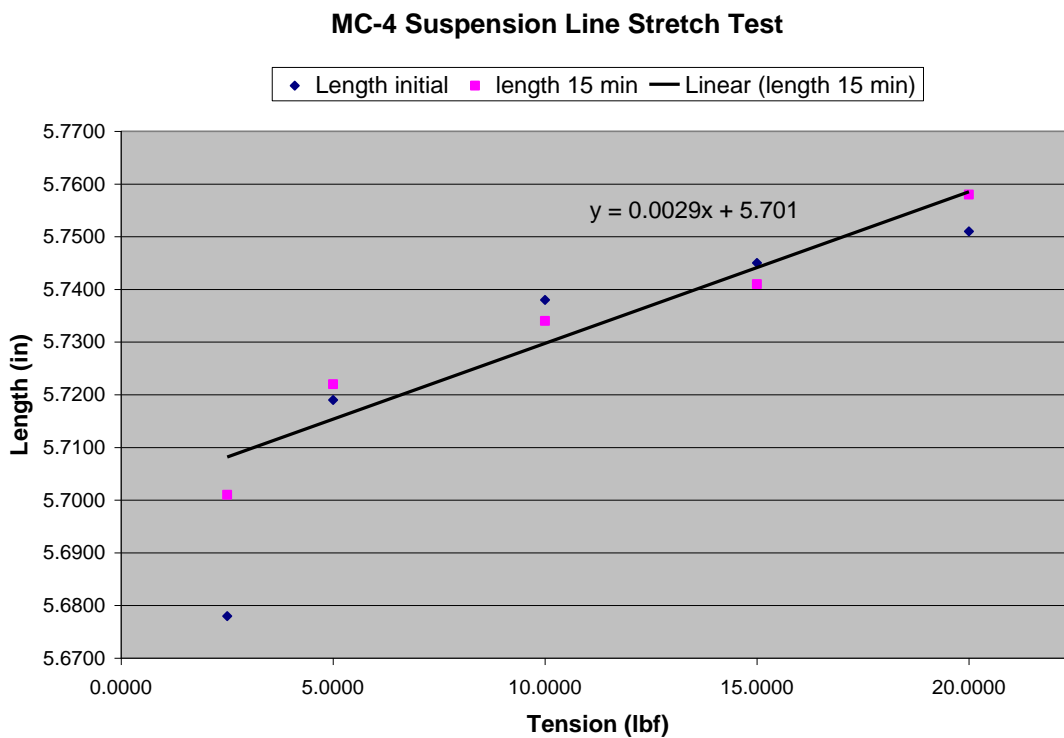
This drawing is submitted solely for the information and exclusive use of the original addressee. It is not to be divulged in whole or in part, by any firm or individual without written permission from FUTEK.

10 THOMAS
IRVINE, CA 92618 USA
1-800-23-FUTEK (38835)

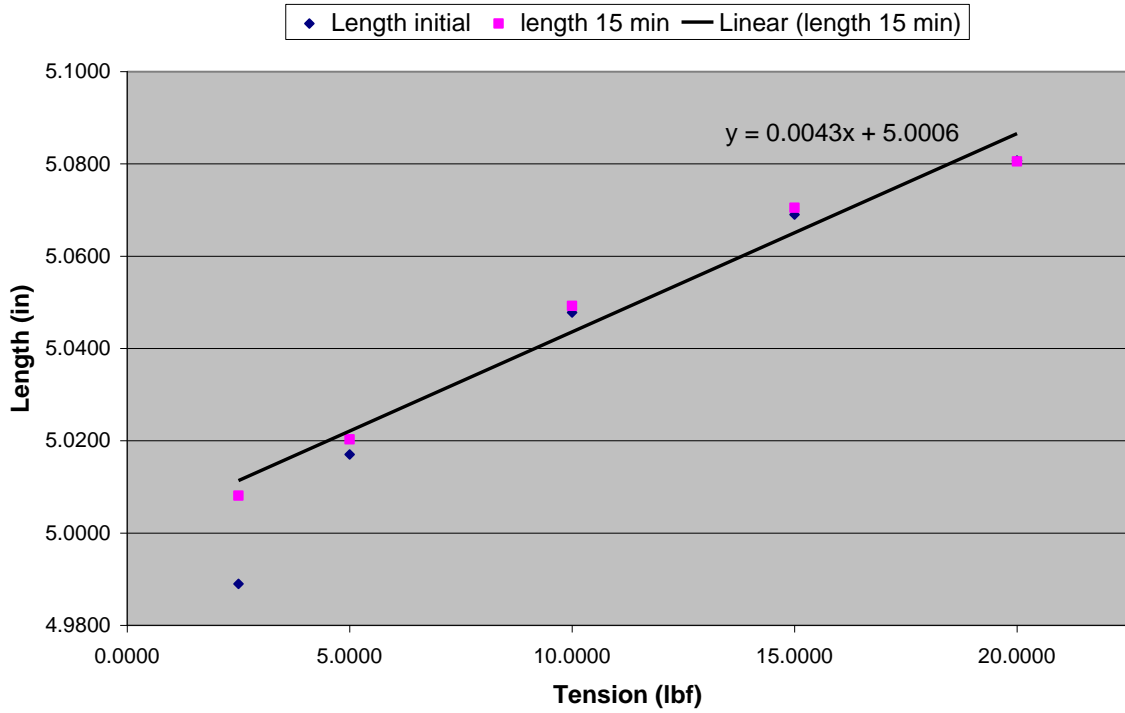
INTERNET:
<http://www.futek.com>

Appendix B – Line Stretch Testing

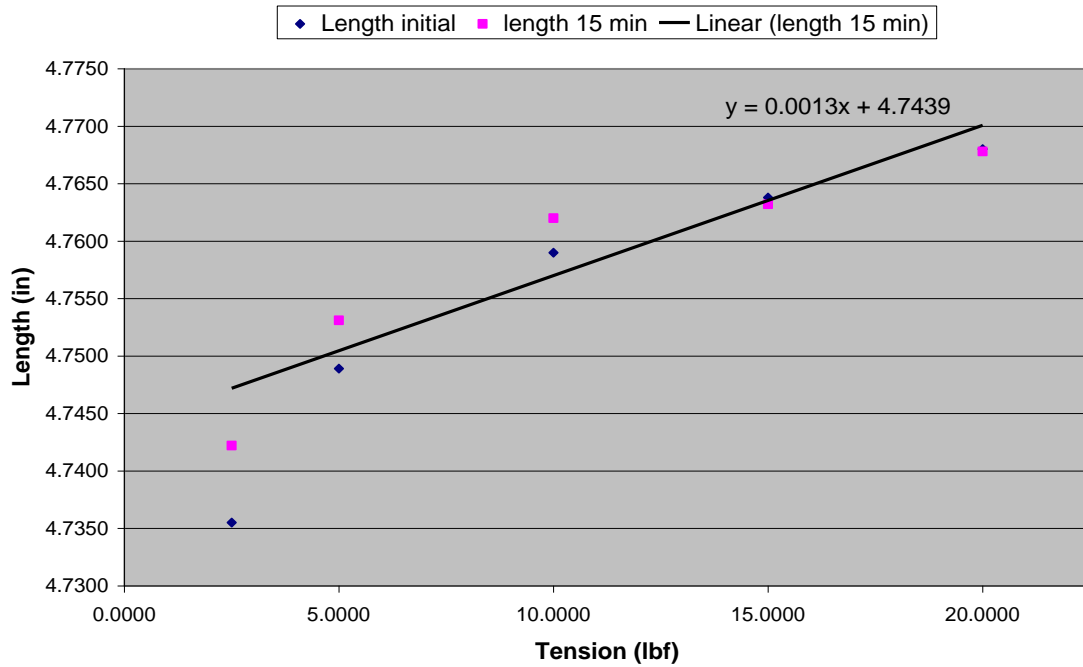
The suspension lines were marked by clamping two staples onto the line at approximately 5 inches apart. These staples were then used as points to measure with the caliper. The following steps were repeated for each strength line: First, 2.5 lbs were hung from the line and a measurement was taken with the caliper. After 15 minutes passed, another measurement was taken. After testing the MC-4, it was determined that allowing a weight to hang for longer than 15 minutes created no significant change in the line length. After 15 minutes, weights were changed to 5 lbs and two readings were taken (one initial, one after 15 min). Lastly, weights were added and two readings were taken for 10, 15, and 20 lbs weights.



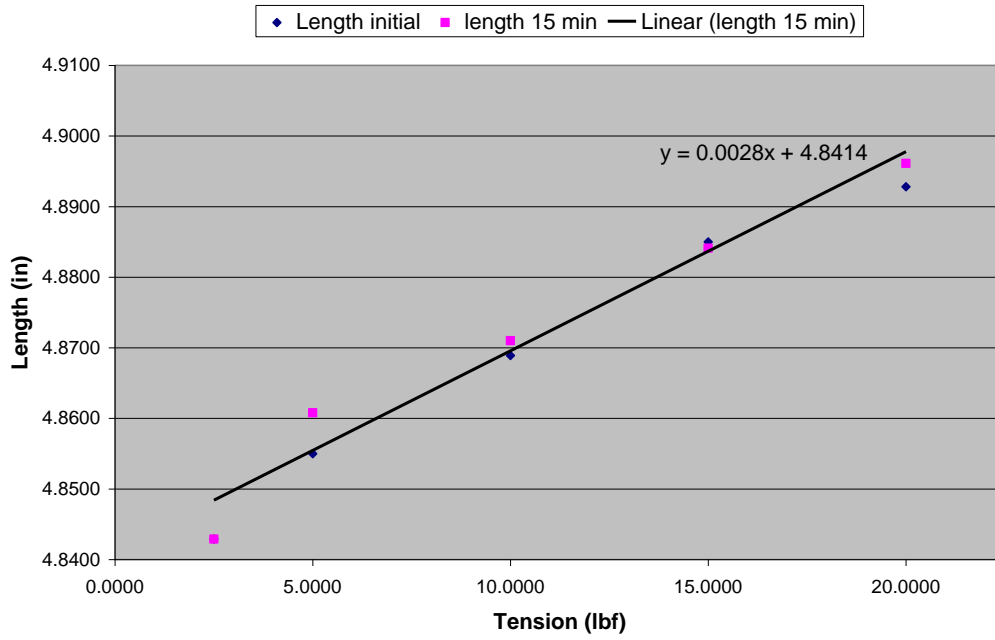
Spectra #2000 Stretch Test



Spectra #4000 Stretch Test

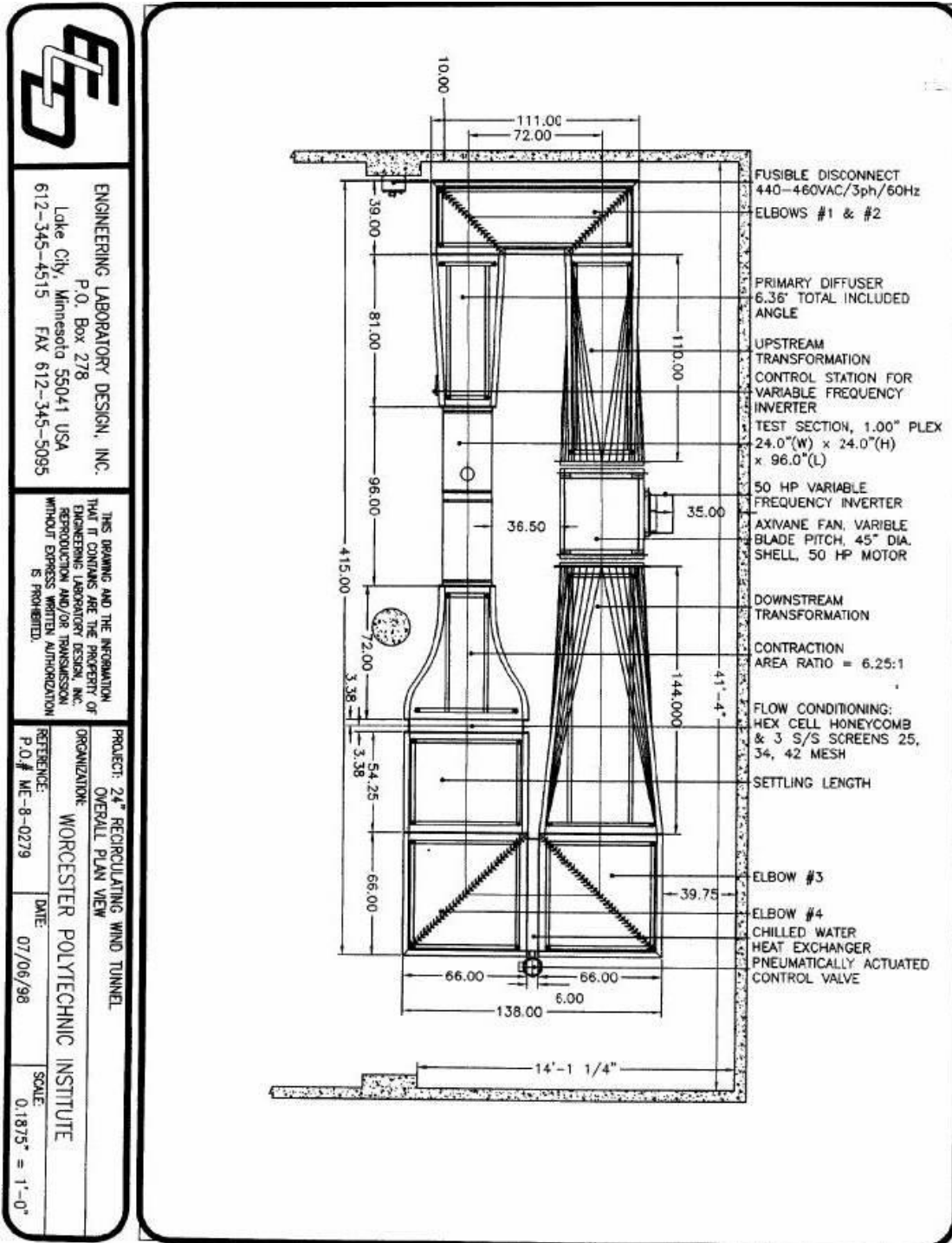


Spectra #6000 Stretch Testing



It was determined from these tests that the parachute suspension lines did not show appreciable tension stretching under loads anticipated in the study.

Appendix C – Wind Tunnel Specifications



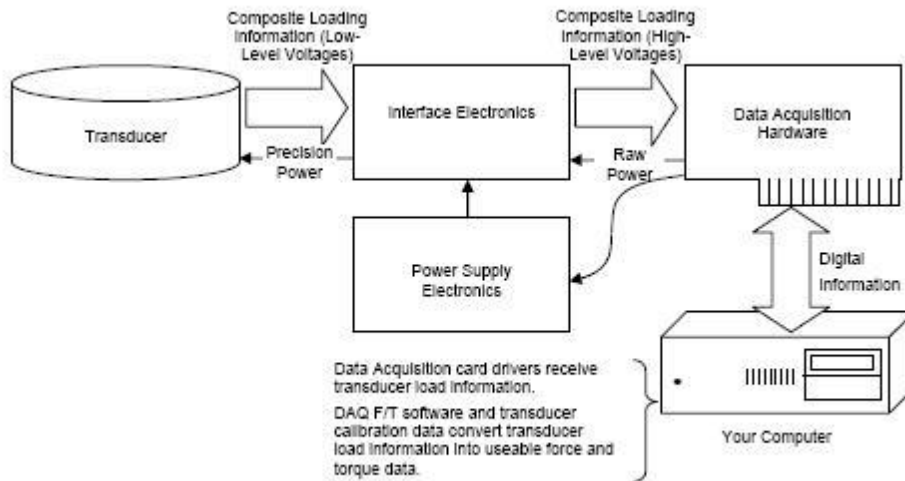
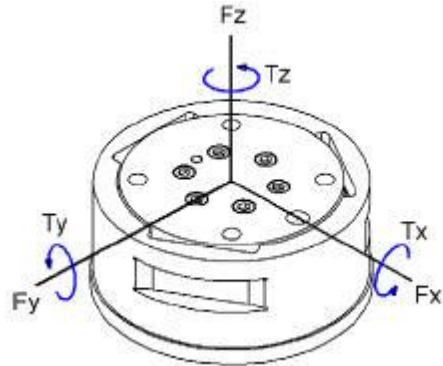
ENGINEERING LABORATORY DESIGN, INC.
 P.O. Box 278
 Lake City, Minnesota 55041 USA
 612-345-4515 FAX 612-345-5095

THIS DRAWING AND THE INFORMATION
 THAT IT CONTAINS ARE THE PROPERTY OF
 ENGINEERING LABORATORY DESIGN, INC.
 REPRODUCTION AND/OR TRANSMISSION
 WITHOUT EXPRESS WRITTEN AUTHORIZATION
 IS PROHIBITED.

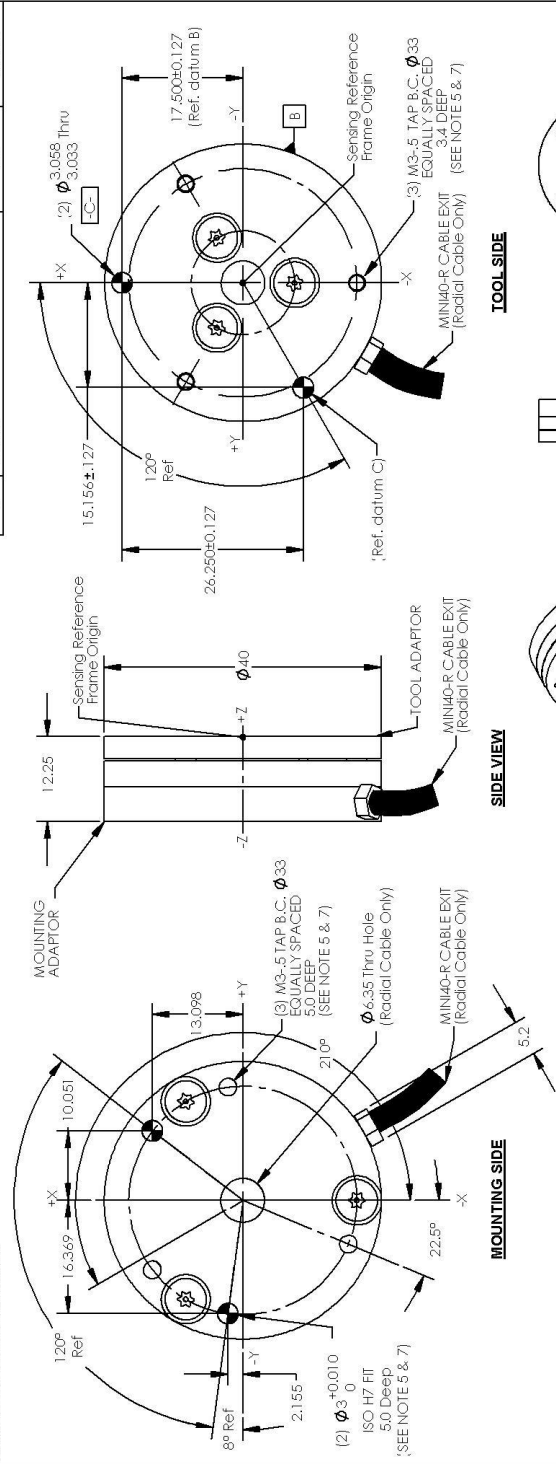
PROJECT: 24" RECIRCULATING WIND TUNNEL
 ORGANIZATION: WORCESTER POLYTECHNIC INSTITUTE
 OVERALL PLAN VIEW

REFERENCE: P.O.# ME-8-0279
 DATE: 07/06/98
 SCALE: 0.1875" = 1'-0"

Appendix D – Transducer Specifications



Rev.	Description	Initiator	Date
01	Initial Issue	DSS	3/27/2006



INDUSTRIAL AUTOMATION 1031 Goodworth Drive, Apex, NC 27339, USA Tel: +1 919 772 0115 Email: info@at-ia.com Fax: +1 919 772 8299 www.at-ia.com ISO 9001 Registered Company	
TITLE	MINI40 Transducer Radial & Axial Cable Exit
CREATED BY	D. Swanson 3/9/06
CHECKED BY	D. Perry 3/9/06
SCALE	2:1
DRAWING NUMBER	9230-05-1278-01
SIZE	B
WEIGHT	
ASSEMBLY REF.	
DATE	
SHEET	OF 1

NOTES: UNLESS OTHERWISE SPECIFIED
 DO NOT SCALE DRAWING. DRAWN IN SOLIDWORKS
 DEBURR AND BREAK ALL SHARP EDGES AS IS
 AVOID EXCESSIVE MACHINING SCRATCHES
 ALL DIMENSIONS ARE IN INCHES UNLESS OTHERWISE SPECIFIED
 ALL DIMENSIONS ARE AFTER ANODIZING
 AND SAAL LER BEFORE ANODIZING
 .XXX DECIMALS ±.001
 .XX DECIMALS ±.010
 .X DECIMALS ±.045
 ANGLES ± 1°
 3RD ANGLE PROJECTION

NOTES:
 1. MINI40 IS AVAILABLE WITH EITHER A RADIAL (MINI40-R) OR AXIAL (MINI40-A) CABLE EXIT.
 2. MOUNTING AND TOOL ADAPTOR MADE OF EITHER ALUMINUM OR SST (CUSTOMER SPECIFIED). TRANSDUCER MADE OF HARDENED STAINLESS STEEL.
 3. USE M3 TAPPED HOLES AND 3MM DOWEL PIN HOLES ON TOOL AND MOUNTING ADAPTOR FOR INTERFACING.
 4. CONNECTOR (NOT SHOWN) HAS 17MM DIAMETER AND IS 67.5MM LONG.
 5. DOWEL PIN LOCATION ±.025mm; MOUNTING SCREW LOCATION ±.125mm
6. WARNING: DO NOT LOOSEN OR REMOVE INTERFACE PLATES DUE TO POTENTIAL DAMAGE TO THE TRANSDUCER.
7. DO NOT EXCEED INTERFACE DEPTH. MAY CAUSE DAMAGE TO THE TRANSDUCER.
8. DO NOT EXCEED INTERFACE DEPTH. MAY CAUSE DAMAGE THROUGH CENTER HOLE TO TOUCH BOTH THE MOUNTING AND TOOL ADAPTER PLATES OR PERFORMANCE WILL BE COMPROMISED.

Appendix E - Transducer Certificate of Calibration



Certificate of Calibration

Serial Number: FT7803
Model: Mini40
Calibration: SI-40-2
Electronics: DAQ
Output Range: +/-10 V

Gain Multiplier: 1

Rated (Full-Scale) Loads:

Fx	Fy	Fz	Tx	Ty	Tz
40 N	40 N	120 N	2 N-m	2 N-m	2 N-m

Measurement Uncertainty (95% confidence level, percent of full-scale load):

Fx	Fy	Fz	Tx	Ty	Tz
1.50%	1.50%	0.75%	1.75%	1.50%	1.50%

The above Measurement Uncertainty values are the maximum amount of error for each axis expressed as a percentage of its full-scale load.

Calibration Temperature: 72° F
Temperature Compensation: hardware

Calibration Date: 12 July 2007
Calibration Interval: 12 months
Calibration Due: 12 July 2008

Date Printed: 12 July 2007

ATI certifies that the above product was calibrated in accordance with applicable ATI procedures. These procedures are compliant with the ISO 9001 standard to ensure that the above product is within ATI specifications. To meet this level of accuracy any loads must be correctly aligned to the transducer origin and the transducer must be mounted to a sufficiently strong surface.

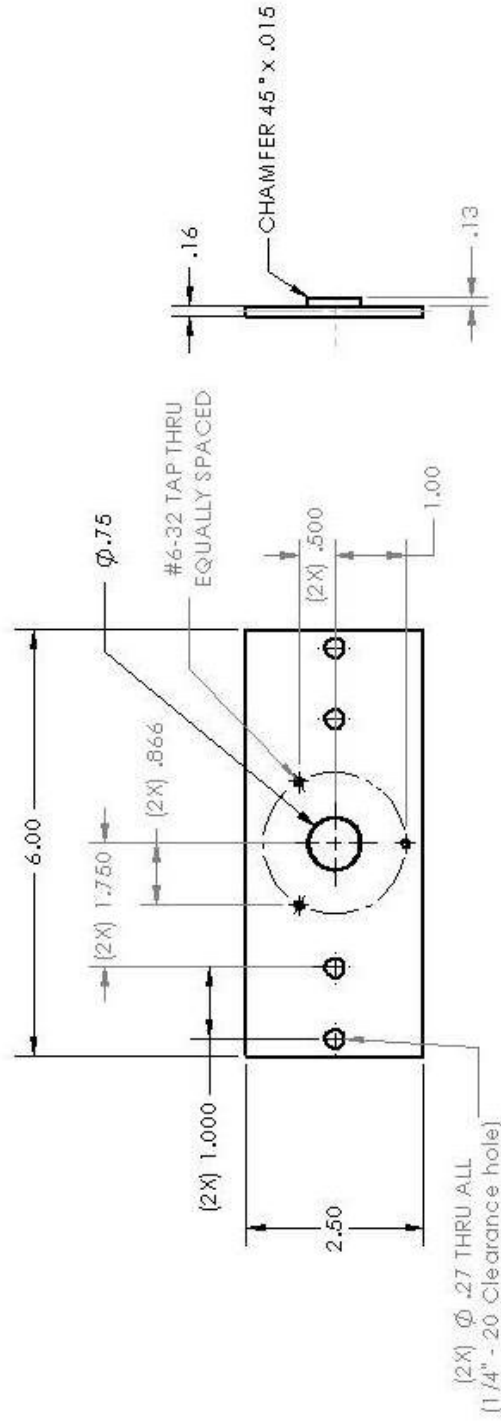
For questions or comments, please contact your ATI representative.

9105-CAL-CERT
Revision 03, December 2003

Engineered Products for Robotic Productivity

Pinnacle Park . 1031 Goodworth Drive, Apex, NC 27539 . Tel: 919.772.0115 . Fax: 919.772.8259 . www.ati-ia.com . E-mail: info@ati-ia.com

Appendix F - Transducer – to – Tensioning Arm Plate



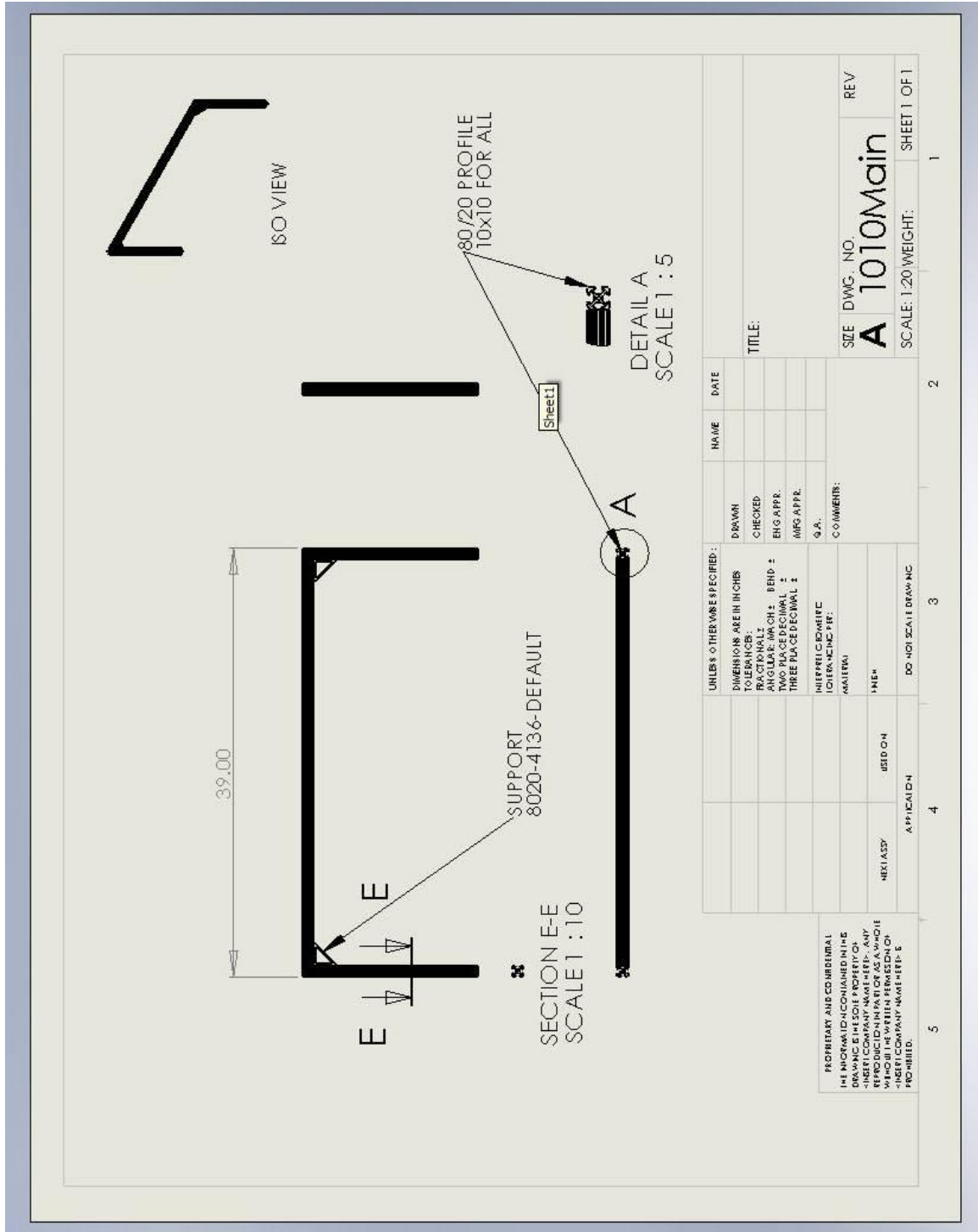
NOTES:
1) BREAK ALL EDGES

UNLESS OTHERWISE SPECIFIED:		NAME	DATE
DIMENSIONS ARE IN INCHES	DRAWN		
FRACTIONS: 1/8, 1/4, 3/8, 1/2, 5/8, 3/4, 7/8, 1, 1 1/8, 1 1/4, 1 1/2, 1 3/4, 1 7/8, 2, 2 1/8, 2 1/4, 2 1/2, 2 3/4, 3, 3 1/8, 3 1/4, 3 1/2, 3 3/4, 4, 4 1/8, 4 1/4, 4 1/2, 4 3/4, 5, 5 1/8, 5 1/4, 5 1/2, 5 3/4, 6, 6 1/8, 6 1/4, 6 1/2, 6 3/4, 7, 7 1/8, 7 1/4, 7 1/2, 7 3/4, 8, 8 1/8, 8 1/4, 8 1/2, 8 3/4, 9, 9 1/8, 9 1/4, 9 1/2, 9 3/4, 10	CHECKED		
ANGULAR: ARC MIN: 5 BEND: 1	ENG APPR.		
FINISH: DECIMAL: 3	AWC APPR.		
THREE PLACE DECIMAL: 3	D.A.		
WRITE UP: DIMENSIONS	COMMENTS:		
WRITE UP: DIMENSIONS			
MATERIAL			
TEMP			
401.430			
APPRECIATION			
DD: 10/12/11 BLANK			
2	3	4	5
1	2	3	4
1	2	3	4
1	2	3	4

PROPRIETARY AND CONFIDENTIAL
INFORMATION COMPARED TO THE
DRAWING IS THE SOLE PROPERTY OF
CIRCMOUNT COMPANY. ANY
REPRODUCTION OR PARTIAL WHOLE
REPRODUCTION WITHOUT THE WRITTEN
PERMISSION OF CIRCMOUNT COMPANY IS
PROHIBITED.

SIZE DWG. NO. REV
A circMount
SCALE: 1:1 WEIGHT: SHEET 1 OF 1

Appendix G – Tensioning Structure



Appendix H – Project Timeline

MQP Work	A Term	B Term	C Term	D Term
Research	✓			
Design	✓			
Writing	✓	✓	✓	✓
Building		✓		
Testing		✓	✓	✓
Analysis			✓	✓

Appendix I – Final Experimental Matrix

BASIC EXPERIMENTAL CALCULATIONS

Line Rotation Angle	Velocity (m/s)	Tension (lbf)	Line Rotation Angle	Velocity (m/s)	Tension (lbf)	Line Rotation Angle	Velocity (m/s)	Tension (lbf)
Parallel (streamlined)	6	0.21	30 Degrees	6	0.21	45 Degrees	6	0.21
		0.744			0.744			
		1.052			1.052			
		1.488			1.488			
	8	0.21		8	0.21		8	0.21
		0.744			0.744			
		1.052			1.052			
		1.488			1.488			
	10	0.21		10	0.21		10	0.21
		0.744			0.744			
		1.052			1.052			
		1.488			1.488			
12	0.21	12	0.21	12	0.21			
	0.744		0.744					
	1.052		1.052					
	1.488		1.488					
60 Degrees	6	0.21	Perpendicular	6	0.21	45 Degrees	6	0.21
		0.744			0.744			
		1.052			1.052			
		1.488			1.488			
	8	0.21		8	0.21		8	0.21
		0.744			0.744			
		1.052			1.052			
		1.488			1.488			
	10	0.21		10	0.21		10	0.21
		0.744			0.744			
		1.052			1.052			
		1.488			1.488			
12	0.21	12	0.21	12	0.21			
	0.744		0.744					
	1.052		1.052					
	1.488		1.488					

Appendix J – Mean Drag Data

Line Rotation Angle	Velocity (m/s)	Tension	Measured Mean Drag, N
Parallel (streamlined)	6	0.21	0.237
		0.744	0.2455
		1.052	0.216
		1.488	0.3424
		2.222	0.1478
	8	0.21	0.3309
		0.744	0.2605
		1.052	0.3447
		1.488	0.3663
		2.222	0.4009
	10	0.21	0.4392
		0.744	0.447
		1.052	
		1.488	
		2.222	
	12	0.21	
		0.744	
		1.052	
		1.488	
		2.222	
Line Rotation Angle	Velocity (m/s)	Tension	Measured Mean Drag, N
Perpendicular	6	0.21	0.6106
		0.744	
		1.052	
		1.488	
		2.222	
	8	0.21	0.7963
		0.744	
		1.052	
		1.488	
		2.222	
	10	0.21	1.105
		0.744	
		1.052	
		1.488	
		2.222	
	12	0.21	1.5876
		0.744	
		1.052	
		1.488	
		2.222	

Appendix K – 80/20 Aluminum Extrusions

Official website - <http://www.8020.net/> - Sections in use for this MQP:

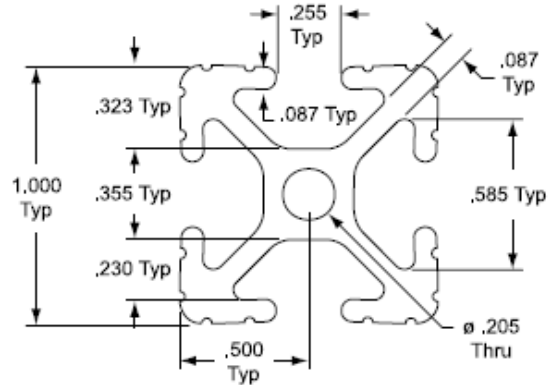
1010 T-Slotted Profile - 10 Series

- Compatible with all 10 Series fasteners
- Four open available T-slots for mounting accessories
- 1010 is ideal for machine guards, sound enclosures, work benches, displays, and panel mount racks




**VIBRATION
PROOF™**

Part No.	1010
Material	6105-T5
Finish	Clear Anodized
Weight Per Foot	.5097 Lbs.
Stock Length (+/- .125")	97" - Part No. 1010-97 145" - Part No. 1010-145 242" - Part No. 1010-242
Moment Of Inertia	IX=.0442" ⁴ IY=.0442" ⁴
Estimated Area	.4379 Sq. In.



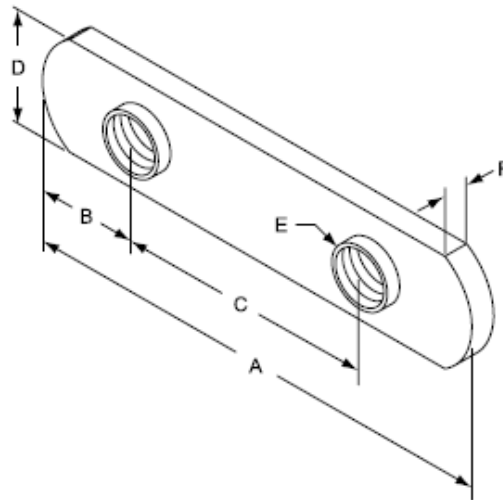
Quick Machining Reference



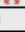
Machining Service	Service Number
Cut to Length	7005 (see page 386)
.218" Access Hole	7051 (see page 388)
Anchor Counterbore	7042 (see page 390)
Tap Profile End	7061 (see page 387)


Note: Look for the  icon throughout the Fractional portion of this catalog. This icon points out all 10 Series compatible parts and accessories.

Double Economy T-Nuts

- Reduces assembly time
- Loads from the profile end only
- Perfect for multiple hole joining plates
- Made from steel with bright and black zinc finishes.
- Refer to pages 101-111 for our full screw and bolt offering

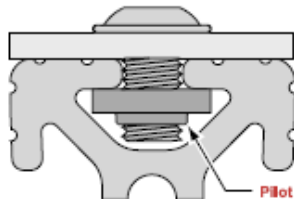


Part No.	A	B	C	D	E (Thread)	F	Finish	Lbs.
3281 	1.375	.187	1.000	.443	8-32	.095	Black Zinc	.019
3280 	1.875	.443	1.000	.443	1/4-20	.095	Black Zinc	.012
3800 	1.870	.443	1.000	.443	M6 x 1.00	.095	Bright Zinc	.012
3279	2.810	.655	1.500	.625	5/16-18	.142	Black Zinc	.063
3879	3.000	.750	1.500	.625	M8 x 1.25	.142	Bright Zinc	.063

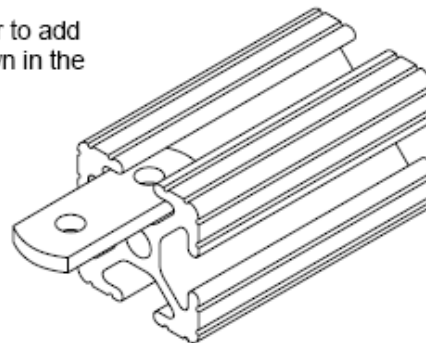
 = 10 Series Compatible Part

Threaded Pilot Projection

The threaded pilot projection provides more thread in order to add strength to the fastener. Always position the projection down in the T-slot to avoid crashing and an uneven connection.



**Pilot Projection
Should Always
Face Down**

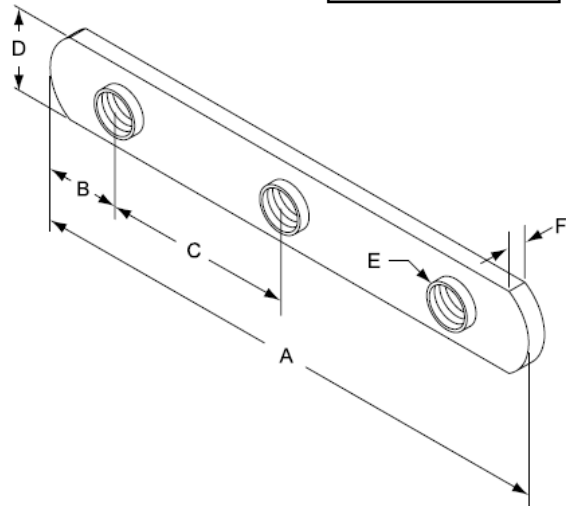
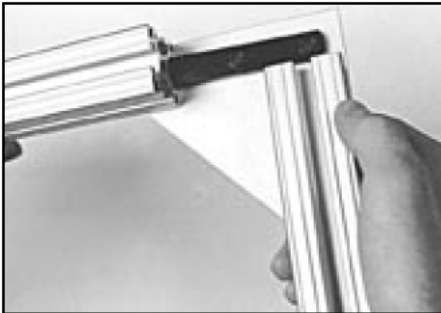
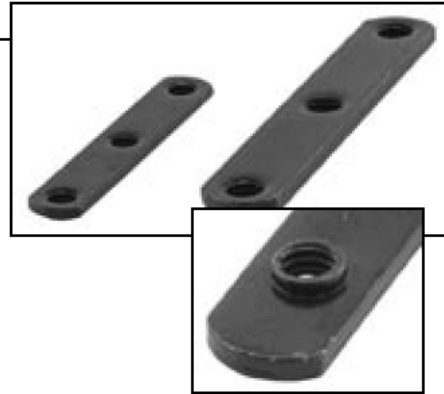


Phone: 260-248-8030 • Fax: 260-248-8029 • www.8020.net

Triple Economy T-Nuts



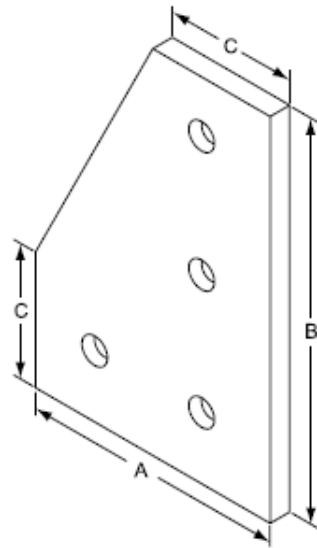
- Reduces assembly time
- Loads from the profile end only
- Made from steel with bright and black zinc finishes
- Perfect for multiple hole joining plates
- Refer to pages 101-111 for our full screw and bolt offering



Part No.	A	B	C	D	E (Thread)	F	Finish	Lbs.
3287	2.450	.241	1.000	.440	1/4-20	.095	Black Zinc	.019
3900	2.450	.241	1.000	.440	M6 x 1.00	.095	Bright Zinc	.020
3285	3.560	.296	1.500	.625	5/16-18	.142	Black Zinc	.063
3805	3.560	.296	1.500	.625	M8 x 1.25	.142	Bright Zinc	.063

= 10 Series Compatible Part

4 Hole 90° Joining Plate



10 Series Recommended Bolt Assembly:

Part No.	Qty	Description
3321	4	1/4-20 x 1/2" FBHSCS & Econ T-Nut

For more 10 Series bolt assembly options, see Table G on page 118.

15 Series Recommended Bolt Assembly:

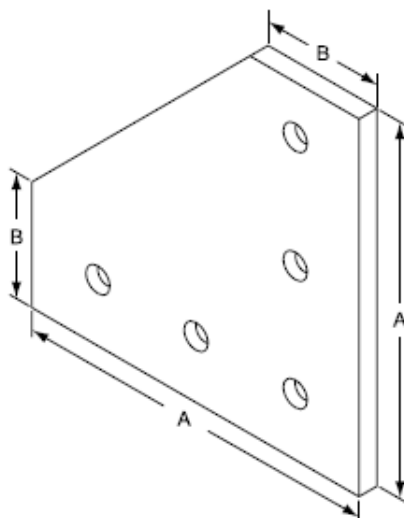
Part No.	Qty	Description
3320	4	5/16-18 x 1 1/16" FBHSCS & Econ T-Nut
OR		
3325	4	5/16-18 x 3/4" Econ. T-Slot Stud, Washer, Hex Nut

For more 15 Series bolt assembly options, see Table C on page 117.

= 10 Series Compatible Part

Part No.	A	B	C	Lbs.
4150	2.000	3.000	1.000	.090
4350	3.000	4.500	1.500	.260

5 Hole 90° Joining Plate



10 Series Recommended Bolt Assembly:

Part No.	Qty	Description
3321	5	1/4-20 x 1/2" FBHSCS & Econ T-Nut

For more 10 Series bolt assembly options, see Table G on page 118.

15 Series Recommended Bolt Assembly:

Part No.	Qty	Description
3320	5	5/16-18 x 1 1/16" FBHSCS & Econ T-Nut
OR		
3325	5	5/16-18 x 3/4" Econ. T-Slot Stud, Washer, Hex Nut

For more 15 Series bolt assembly options, see Table C on page 117.

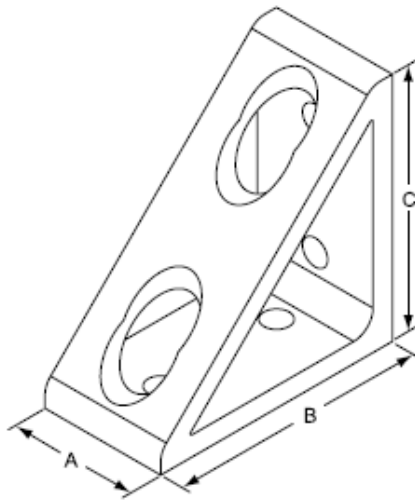
= 10 Series Compatible Part

Part No.	A	B	Lbs.
4151	3.000	1.000	.125
4351	4.500	1.500	.370

4 Hole Inside Gusset Corner Bracket



↑↓
Page 85



10 Series Recommended Bolt Assembly:

Part No.	Qty	Description
3393 ☞	4	1/4-20 x 1/2" BHSCS & Econ T-Nut

For more 10 Series bolt assembly options, see Table M on page 119.

15 Series Recommended Bolt Assembly:

Part No.	Qty	Description
3320	4	5/16-18 x 1 1/16" FBHSCS & Econ T-Nut

For more 15 Series bolt assembly options, see Table N on page 120.

☞ = 10 Series Compatible Part

Part No.	A	B	C	Lbs.
4136 ☞	.875	2.000	2.000	.092
4336	1.310	3.000	3.000	.275

Appendix L – MC-4 Parachute Technical Specifications

TECHNICAL SPECIFICATIONS

Canopy Area:	370 sq ft
Span:	28.5 ft (8.7m)
Chord:	13.0 ft. (4.0m)
L/D:	3 to 1
Maximum Suspended Weight:	360 lbs. (182 kg)
Forward Speed Range:	10-25 mph (24-40 km/hr)
ROD Full Flight:	14-16 fps (4.3 – 4.9 m/sec)
ROD 50% Brakes:	6-10 fps (1.8 – 3.1 m/sec)
ROD 100% Brakes:	2-6 fps (0.6 – 1.8 m/sec)
Maximum Deployment Height:	25,000 ft MSL (7700 m)
Deployment Velocity:	0 to 150 KIAS



Appendix M – WPIConversion08.m MATLAB code

```
% WPIConversion08
% Takes raw and bias data from labview (.csv format), subtracts bias and
% converts to forces and torques. Outputs .mat and .txt files.
% Used in conjunction with ATIDaqFT_Convert2.m SB '08

clear; clc;
% Read raw data
[filename, pathname] = uigetfile('*.csv', 'Select raw data file (must be in the
current matlab directory)');
if filename ~=0
    F = csvread(filename, 5, 0);
    ait=F(:,1); ai0=F(:,2); ai1=F(:,3); ai2=F(:,4);
    ai3=F(:,5); ai4=F(:,6); ai5=F(:,7);
    RawData = [ai0, ai1, ai2, ai3, ai4, ai5];
else
    return;
end

%Load BiasData Matrix
[file, path] = uigetfile('*.csv', 'Select bias data file or cancel for none');
if file ~= 0;
    FB = csvread(file, 5, 0);
    Biasai1=FB(:,1); Biasai0=FB(:,2); Biasai1=FB(:,3); Biasai2=FB(:,4);
    Biasai3=FB(:,5); Biasai4=FB(:,6); Biasai5=FB(:,7);
    BiasData = [Biasai0, Biasai1, Biasai2, Biasai3, Biasai4, Biasai5];
    data = input('Calibration number 1 or 2?');
    if data==1
        data = ATIDaqFT_Convert1(RawData(:, 1:6), BiasData);
    else
        data = ATIDaqFT_Convert2(RawData(:, 1:6), BiasData);
    end
else
    data = input('Calibration number 1 or 2?');
    if data==1
        data = ATIDaqFT_Convert1(RawData(:, 1:6));
    else
        data = ATIDaqFT_Convert2(RawData(:, 1:6));
    end
end

% Save data to a Matlab file
Data = [ait data];
[file, path] = uigetfile('*.mat', 'Select file to save');
HeaderNames = {'Time (s)', 'Fx (N)', 'Fy (N)', 'Fz (N)', 'Tx (N-m)', 'Ty (N-
m)', 'Tz (N-m)'};
save([path file], 'HeaderNames', 'Data');

% Save data to a text file
if(file~=0)
    file2 = [file '.txt'];
    titles = ['Time (s)\t', 'Fx (N)\t', 'Fy (N)\t', 'Fz (N)\t', 'Tx (N-m)\t',
'Ty (N-m)\t', 'Tz (N-m)\n'];
    fid = fopen([path file2], 'w');
    fprintf(fid, titles);
    fprintf(fid, '%f\t%f\t%f\t%f\t%f\t%f\t%f\n', Data);
    fclose(fid);
end
```

Appendix N – ATIDaqFT_Convert2.m MATLAB code

```
function [data, varargout] = ATIDaqFT_Convert2(varargin)
% ATIDAQ_CONVERT2
%   Converts raw measured voltage from a ATI Industrial Automation
%   force/torque transducer and converts it to data with real units based
%   on a calibration performed at the factory. See notes below with
%   conversion matrix about calibration procedures and units.
%
% DATA = ATIDAQFT_CONVERT(RAWDATA)
%   The rawdata matrix should be in a m x n matrix where m = the length of the data
%   and n is the number of channels (in this case n should equal 6). So for example,
%   if we collected 4 data points each on of six channels, the matrix would look like
%       rawdata = [a1 a2 a3 a4 a5 a6;
%                  b1 b2 b3 b4 b5 b6;
%                  c1 c2 c3 c4 c5 c6;
%                  d1 d2 d3 d4 d5 d6];
%
% DATA = ATIDAQFT_CONVERT(RAWDATA, BIASDATA)
%   If there is bias data to subtract from the measurements, the biasdata
%   matrix should be a 1 x n matrix (a row vector) where each column represents
%   the bias for its corresponding channel. If the biasdata matrix is p x n,
%   then the mean value for each column is calculated and used as the bias for
%   that channel.
%
% DATA = ATIDAQFT_CONVERT(RAWDATA, BIASDATA, WORKINGMATRIX)
%   The WORKINGMATRIX array is a 6 x 6 matrix used to convert the raw voltage
%   measurements to real units.
%=====
%===== Transducer Specific =====
% The working matrix was generated in the Excel spreadsheet 'DAQ FT Manual
% Calculations.xls' based on the calibration file 'FT5418.cal' with a
% calibration date of 11/19/2003. This matrix will be valid until the
% force/torque transducer is sent back to ATI Industrial Automation for
% re-calibration.
%
% Transducer Specifications:
%   Serial# FT5418
%   Body Style: Mini40
%   Part#: SI-20-1
%   Calibration Date: 11/19/2003
%   Force Units: N
%   Torque Units: N-m

ForceUnits = 'N';
TorqueUnits = 'N-m';
%WorkingMatrix = [-0.079636876  2.830384366  0.015076630  0.006271499  0.024385780 -2.757029983;
%                 0.055397396 -1.651787361  0.060351339  3.050951534 -0.023779434 -1.542305896;
%                 -4.878950415  0.176097067 -4.791209036  0.242878384 -4.815770952  0.173818343;
%                 0.068922137 -0.009858819 -0.000337191  0.015719643 -0.068803532 -0.006324293;
%                 -0.038500074 -0.012992899  0.078428653 -0.003789350 -0.038973169  0.015288241;
%                 -0.000968989  0.038723948  0.000218005  0.036897074 -0.000404944  0.038308076];

% Transducer Specifications:
%   Serial# FT5418
%   Body Style: Mini40
%   Part#: SI-20-1
%   Calibration Date: 2007 calibration
%   Force Units: N
%   Torque Units: N-m

%WorkingMatrix = [-0.171556748  6.040214206  0.035046957  0.027619155  0.044889995 -5.95368107;
%                 %0.116094571 -3.527273873  0.113758948  6.671261219 -0.047265031 -3.335328705;
%                 %-10.32801247  0.365961288 -10.14937444  0.518405937 -10.3562331  0.398920555;
%                 %0.147166468 -0.024564795  0.003060397  0.036257793 -0.145617297 -0.012329634;
```



```

%-0.082355848 -0.029600994 0.165958261 -0.008531483 -0.081312323 0.034982476;
%-0.000550803 0.083515552 0.001125769 0.080623143 -3.92386E-05 0.080874304];

% Transducer Specifications:
% Serial# FT5418
% Body Style: Mini40
% Part#: SI-40-2
% Calibration Date: 2007 calibration
% Force Units: N
% Torque Units: N-m

WorkingMatrix = [-0.166365575 6.046196071 0.039009271 0.024620525 0.05702225 -5.954128093;
0.116655719 -3.530225937 0.115044402 6.667266024 -0.052260425 -3.328114703;
-10.31232427 0.361564313 -10.13659083 0.53045633 -10.33441926 0.391446016;
0.148349573 -0.024199681 0.003322994 0.036387055 -0.145022835 -0.012902577;
-0.082868206 -0.029621496 0.165589829 -0.008469382 -0.081894771 0.03503978;
-0.00143718 0.082692707 0.000166796 0.080768232 -0.00093295 0.08101238];

%=====
%=====
narg = nargin;
if narg == 1
    rawdata = varargin{1};
    biasdata = zeros(size(rawdata));
elseif narg == 2
    rawdata = varargin{1};
    biasdata = varargin{2};
    [m,n] = size(rawdata);
    [p,n] = size(biasdata);
    if p > 1
        biasdata = mean(biasdata);
    end
    biasdata = repmat(biasdata, m,1);
elseif narg == 3
    rawdata = varargin{1};
    biasdata = varargin{2};
    [m,n] = size(rawdata);
    [p,n] = size(biasdata);
    if p > 1
        biasdata = mean(biasdata);
    end
    biasdata = repmat(biasdata, m,1);
    WorkingMatrix = varargin{3};
else
    error('Incorrect number of input arguments.');

```

Appendix O – NEW_MQP_FFT.m MATLAB code

```
% NEW_MQP_FFT.m
% US Army Soldier Center, Natick MA MQP
% A '07 - D '08
% Fourier Transform and Filtering Analysis code package
% SB'08

clear; close; clc

Forces = load (uigetfile('Select appropriate .mat file'));
c=input('Perform fast-fourier on which column? 2=Fx, 3=Fy, 4=Fz, 5=Tx,
6=Ty, 7=Tz:');
y = Forces.Data(:,c); % This identifies column (2-7 ~ Fx-Tz)
Fs = 5000; % Sampling Frequency (How many times per second)
d=1/Fs; % Sampling time
t=0:d:(length(y)-1)*d; % Time Step
z=abs(fft(detrend(y)))/length(y); % Fast-Fourier Transform Function,
divide by length to preserve energy, detrend eliminates dc
s=2*z(1:length(y)/2); % First half of Column z data points, multiplied
by 2 for conservation of energy
power=s.^2;
df=Fs/length(z); % Fourier Frequency Resolution
f=0:df:df*(length(s)-1); % Frequency step

% Plot of Force Vs. Time
figure, plot(t,y), ylabel('Force (N)'), xlabel('Time (s)'),grid on,
title('Force Data')

% Plot of Power vs. frequency
figure,plot(f,power), ylabel('Power'),xlabel('Frequency
(Cycles/s)'),grid on, title('Periodogram')

% Plot of Power vs. period
figure,period = 1./f; plot(period,power),grid
on,ylabel('Power'),xlabel('Period(s/Cycle)'), title('Power vs. Period')

Mean_Force = mean(y)
Standard_Deviation = std(y)
```